SANDIA REPORT
SAND2003-8598
Unlimited Release
Printed October 2003

Uncertainty Quantification in Reacting Flow Modelling

H.N. Najm, M.T. Reagan, O.M. Knio, R.G. Ghanem, and O.P. Le Maître

Prepared by
Sandia National Laboratories
Albuquerque, New Mexico 87185 and Livermore, California 94550

Sandia is a multiprogram laboratory operated by Sandia Corporation, a Lockheed Martin Company, for the United States Department of Energy's National Nuclear Security Administration under Contract DE-AC04-94AL85000.

Sandia National Laboratories

Issued by Sandia National Laboratories, operated for the United States Department of Energy by Sandia Corporation.

Available to DOE and DOE contractors from
U.S. Department of Energy
Office of Scientific and Technical Information
P.O. Box 62
Oak Ridge, TN 37831

Telephone: (865)576-8401
Facsimile: (865)576-5728
E-Mail: reports@adonis.osti.gov
Online ordering: http://www.doe.gov/bridge
Available to the public from
U.S. Department of Commerce
National Technical Information Service
5285 Port Royal Rd
Springfield, VA 22161

Telephone: (800)553-6847
Facsimile: (703)605-6900
E-Mail: orders@ntis.fedworld.gov
Online order: http://www.ntis.gov/help/ordermethods.asp?loc=7-4-0#online

SAND2003-8412

SAND2003-8598
Unlimited Release
Printed October 2003

Uncertainty Quantification in Reacting Flow Modeling

H.N. Najm, M.T. Reagan,
Sandia National Laboratories
Livermore, CA

O.M. Knio, R.G. Ghanem,
The Johns Hopkins University
Baltimore, MD

and

O.P. Le Maître
Université d'Evry Val d'Essonne
Evry, France

Abstract

Uncertainty quantification (UQ) in the computational modeling of physical systems is important for scientific investigation, engineering design, and model validation. In this work we develop techniques for UQ based on spectral and pseudo-spectral polynomial chaos (PC) expansions, and we apply these constructions in computations of reacting flow. We develop and compare both intrusive and non-intrusive spectral PC techniques. In the intrusive construction, the deterministic model equations are reformulated using Galerkin projection into a set of equations for the time evolution of the field variable PC expansion mode strengths. The mode strengths relate specific parametric uncertainties to their effects on model outputs. The non-intrusive construction uses sampling of many realizations of the original deterministic model, and projects the resulting statistics onto the PC modes, arriving at the PC expansions of the model outputs. We investigate and discuss the strengths and weaknesses of each approach, and identify their utility under different conditions. We also outline areas where ongoing and future research are needed to address challenges with both approaches.

1 Introduction

Confidence intervals on predicted system behavior are necessary for design and optimization of engineering systems. They are also useful from a scientific point of view, where model validation with respect to experimental measurements requires careful measures of uncertainty in both experimental data and computational predictions. In general, uncertainty in computational results can be due to both model and parametric uncertainty. The present work deals with the latter. Empirical physical parameters used in the construction of computational models are inherently uncertain as a result of unavoidable experimental measurement errors. We seek to develop techniques to quantify propagation of this parametric uncertainty, with a focus on detailed, stiff, chemical kinetics.

In general, the propagation of parametric uncertainty can be studied using Monte Carlo (MC) simulations by sampling assumed or known distrubutions of model parameters over many iterations. For complex models that consume considerable computational resources, this method may be very costly and inefficient. Also, this approach does not readily provide information about the sensitivity of model outputs to specific parametric uncertainties. Further, conventional sensitivity analysis sheds some light on first-order parametric dependencies, but does not propagate nonlinear interactions through the model of interest.

An alternate approach is discussed here, based on a spectral stochastic description of uncertain parameters and field quantities using polynomial chaos (PC) expansions for the stochastic representation of uncertainty. Polynomial chaos [1–7] is a member of the set of homogeneous chaos, first defined by Wiener [1]. Ghanem and Spanos [7] implemented a spectral PC expansion in terms of Hermite polynomials of Gaussian basis functions in a finite element method. This was applied in the modeling of transport in porous media [8], solid mechanics [9, 10] and structural [11] applications. The utility of the Hermite-Gaussian PC for modeling non-Gaussian processes was also investigated in [12, 13]. Le Maître *et al.* [14, 15] extended the application of these techniques to thermo-fluid applications in the context of low Mach number flow. Xiu *et al.* [16] used generalized PC [17] for stochastic UQ in the modeling of flow-structure interactions, and for diffusion problems [18]. Debusschere *et al.* [19, 20] used PC for UQ in the context of electrochemical flow in microfluidic systems. Reagan *et al.* [21] studied UQ in the context of chemically reacting H_2-O_2 flow.

In the most basic application, using MC sampling of the stochastic parameters, the corresponding solutions of the deterministic system are evaluated and projected onto the PC basis to compute the spectral mode coefficients. These coefficients are then used to construct probability density functions (PDFs) of the solution, to infer sensitivity to various parametric uncertainties, and to highlight the dominant sources of uncertainty. This non-intrusive spectral projection (NISP) approach [11, 15, 21], has the advantage of being applicable to legacy codes, which are run with varying parameters to compute the statistics and spectral mode values.

For computationally intensive problems, large-scale Latin-Hypercube MC sampling [22] of many deterministic runs may not be practical. For example, studying homogeneous ignition, using a reduced model of 8 uncertain reaction rate preexponentials and five uncertain enthalpies of formation, requires over to 20,000 individual deterministic evaluations of the model to adequately sample the full stochastic space and reach convergence [21]. Increasing the order of the PC expansion to more accurately represent the resultant output PDFs and/or study larger sets of uncertain parameters can dramatically increase the number of samples required to achieve convergence. More complex models containing a greater number of reactions increase both the required sampling and the time required to compute individual realizations. As a result, more complex problems demand a more efficient approach.

An "intrusive" spectral/pseudospectral methodology allows the direct incorporation of spectral stochastic information into the basic formulation of the model. If it is possible to reformulate the governing equations for a particular problem, numerical efficiency can be gained by creating a purpose-built spectral code. In general, these implementations of spectral PC expansions involve (1) the introduction of a new stochastic dimension for each uncertain parameter in the problem, (2) the expansion of parameters and field quantities using PC in terms of these stochastic dimensions, (3) the substitution of these expansions in the governing equations and their reformulation using a Galerkin projection procedure into equations for the stochastic mode strengths, and (4) the solution of this larger system of equations and the reconstruction of the field quantities of the solution based on their PC expansions in terms of the computed stochastic modes. The computational effort required to solve this system can be many times smaller than that required to generate many MC realizations, depending on system nonlinearities and the necessary spectral order.

It is important to note that, while polynomial chaos-based uncertainty quantification provides sensitivity

information, it actually goes well beyond sensitivity analysis to propagate the full probablistic representation of the model inputs to the model outputs. Depending on the chosen order of the PC expansion, intrusive spectral methods also provide *higher-order* sensitivity information. Higher-order effects are not lumped into a single coefficient, but are considered independently and in terms of parameter-parameter interactions. The result is a complete polynomial chaos representation of the complex system response.

The present report presents advances in the state of the art of UQ in both the non-intrusive and intrusive areas as applied to computations of reacting flow. We begin by presenting the essential details of the spectral/pseudo-spectral stochastic polynomial chaos formulation that forms the basis of both approaches. We then present the construction of the non-intrusive approach and discuss results pertaining to non-intrusive UQ in zero-dimensional and one-dimensional reacting flow computations. This is followed by an exposition of the intrusive approach, with associated application to zero-dimensional reacting flow and simpler ODE model problems, and discussion of corresponding results. We finish with conclusions regarding the state of the research in this area and potential future avenues of investigation.

2 Formulation

2.1 Spectral methodology

As mentioned above, this method addresses parametric uncertainty. One can describe an uncertain model parameter as a stochastic quantity with a known PDF. Let an uncertain parameter λ be empirically given by

$$\lambda = \bar{\lambda} \pm \hat{\lambda} \tag{1}$$

where $\bar{\lambda}$ is the mean and $\hat{\lambda}$ defines the range of uncertainty.

With no additional information, we can assume that λ is sampled from a Gaussian PDF with a mean λ_0 and a standard deviation λ_1 consistent with Eq. 1. Further, if we let ξ be a normalized Gaussian variable with zero mean and unit variance we can express λ as the expansion

$$\lambda = \lambda_0 + \xi\lambda_1 \tag{2}$$

If, on the other hand, additional physical constraints are in effect, e.g. when λ is a pre-exponential Arrhenius rate constant that is strictly positive, then a lognormal distribution is necessary. In this case, as discussed in [12, 13] and section 4.1.4, λ can be expanded in powers of ξ, with the necessary order dictated by the skewness of the distribution.

For a general prescribed distribution of λ, satisfying specific conditions [23], we can represent λ as a spectral expansion in terms of suitable orthogonal eigenfunctions with weights associated with a particular density. A well-studied example is the Wiener process (Brownian motion) which can be written as a spectral expansion in terms of HERMITE polynomials and a normal Gaussian distribution. Other examples include Charlier polynomials and the Poisson distribution, and the Laguerre polynomials and the Gamma distribution [23]. In the present context, these spectral expansions are generally referred to as Polynomial Chaos (PC) expansions, following Wiener [1], and focus will be exclusively on the HERMITE-GAUSS PC. Moreover, while these expansions are infinite series, this work will consider only PC expansions truncated at some suitably high order.

A parameter λ can be represented using the (truncated) PC expansion as,

$$\lambda = \sum_{k=0}^{P} \lambda_k \Psi_k \tag{3}$$

where the Ψ_k's are the orthogonal Hermite polynomial functions of ξ [7], such that

$$\Psi_k = \begin{cases} 1 & k = 0 \\ \xi & k = 1 \\ \xi^2 - 1 & k = 2 \\ \cdots & \end{cases} \tag{4}$$

and the λ_k's are the known spectral mode strengths for the PC expansion for λ.

More generally, for N_{dim} uncertain parameters, each parameter introduces a stochastic dimension ξ, such that, with $\theta = \{\xi_1, \xi_2, \cdots, \xi_{N_{\text{dim}}}\}$,

$$\Psi_k = \Psi_k(\theta) = \Psi_k(\xi_1, \xi_2, ..., \xi_{N_{\text{dim}}}), \quad k = 0, \ldots, P. \tag{5}$$

Up to second order ($N_{\text{ord}} = 2$), these polynomials are given by:

$$\Psi_k = \begin{cases} 1 & k = 0 \\ \xi_k & k = 1 \ldots N_{\text{dim}} \\ \xi_m \xi_n - \delta_{nm} & k = N_{\text{dim}} + 1 \ldots P;\ m = 1 \ldots N_{\text{dim}};\ n = 1 \ldots N_{\text{dim}}, \end{cases} \tag{6}$$

they are orthogonal with respect to an inner product,

$$< \Psi_i \Psi_j > \equiv \int \cdots \int \Psi_i(\theta) \Psi_j(\theta) g(\xi_1) \cdots g(\xi_N) d\xi_1 \cdots d\xi_N \tag{7}$$

where

$$g(\xi) = \frac{e^{-\xi^2/2}}{\sqrt{2\pi}} \tag{8}$$

is a Gaussian measure, $< \Psi_i >= \delta_{i0}$, and

$$< \Psi_i \Psi_j >= 0, \quad i \neq j, \quad i > 0,\ j > 0 \tag{9}$$

Note that, in general [17], $P + 1 = (N_{\text{dim}} + N_{\text{ord}})/(N_{\text{dim}}! N_{\text{ord}}!)$.

Using the above orthogonality, it is easy to show, starting with the PC expansion for a general parameter λ in Eq. 3 above, multiplying both sides by Ψ_i and taking inner products, that

$$\lambda_i = \frac{< \lambda \Psi_i >}{< \Psi_i^2 >}, \quad i = 0, \ldots, P \tag{10}$$

Using this formalism, any stochastic field variable $\Phi(x,t)$ can also be represented using the PC expansion, as:

$$\Phi = \sum_{k=0}^{P} \Phi_k(x,t) \Psi_k \tag{11}$$

where the Φ_k's are the *unknown* spectral modes of Φ, analogous to the known spectral modes of λ. Again, given the orthogonality of the Ψ_k's, the Φ_k's are given by

$$\Phi_k = \frac{\langle \Phi \Psi_k \rangle}{\langle \Psi_k^2 \rangle}, \quad k = 0, \ldots, P. \tag{12}$$

The Galerkin projection in Eq. 12 can be used in non-intrusive UQ analysis to project multiple realizations of a deterministic system onto the PC basis [21], as discussed in section 3 below. These projection operations are also the basis for intrusive UQ based on reformulating the governing equations, as in section 4 below. Such a reformulated model construction provides built-in spectral stochastic uncertainty information, and eliminates the need for extensive Monte Carlo sampling of a deterministic problem for UQ purposes. Instead, the extended system of $k = 0, \ldots, P$ governing equations can be solved with an increase in computational load by a factor proportional to $P + 1$.

For a simple example of full spectral reformulation, consider an ODE in terms of Φ and parameter λ:

$$\frac{d\Phi}{dt} = \lambda \Phi, \qquad \Phi(0) = \Phi_0 \tag{13}$$

We can substitute the expansions Eq. 3 and Eq. 11 into the ODE, and rearrange:

$$\sum_{k=0}^{P} \frac{d\Phi_k}{dt} \Psi_k = \sum_{p=0}^{P} \sum_{q=0}^{P} \lambda_p \Phi_q \Psi_p \Psi_q \tag{14}$$

Then, multiplying both sides by Ψ_i, and taking inner products, use the orthogonality between the basis functions to isolate the Ψ's:

$$\frac{d\Phi_i}{dt} = \sum_{p=0}^{P}\sum_{q=0}^{P} \lambda_p \Phi_q \frac{\langle \Psi_p \Psi_q \Psi_i \rangle}{\langle \Psi_i^2 \rangle}, \quad i = 0, \ldots, P \tag{15}$$

where the $C_{pqi} = \langle \Psi_p \Psi_q \Psi_i \rangle / \langle \Psi_i^2 \rangle$ are precomputed coefficient tensors.

Solving for the spatiotemporal evolution of these modes allows the reconstruction of $\Phi(x,t)$ per Eq. 11. This approach requires extensive and specific recoding of an existing code, which can be difficult. For multiple stochastic parameters and field variables, and high non-linearities, evaluation of the multi-dimensional summations and coefficient tensors become intractable (see section 4.1.2). Moreover, there is no evident means of dealing with non-polynomial functions of stochastic quantities within this fully spectral context. These difficulties are resolved using a pseudospectral construction, where order-$2P$ PC expansions resulting from pairwise products of order-P stochastic quantities are reprojected onto an order-P polynomial before proceeding further. This retains the order-P accuracy of the construction, while providing great simplification of the implementation. This construction is discussed in the following section.

2.2 Pseudospectral formulation

In this formulation, a PC-product term involving more than two factors is evaluated using two-factor pseudospectral products. Let

$$w = \lambda u v, \quad u = \sum_{k=0}^{P} u_k \Psi_k, \text{ as well as } \lambda \ \& \ v. \tag{16}$$

Project each two-factor product onto a $(P+1)$ polynomial:

$$\tilde{w} = uv \quad \Rightarrow \quad \tilde{w}_i = \sum_{j=0}^{P}\sum_{k=0}^{P} u_k v_j \frac{\langle \Psi_k \Psi_j \Psi_i \rangle}{\langle \Psi_i^2 \rangle} \tag{17}$$

$$w = \lambda \tilde{w} \quad \Rightarrow \quad w_i = \sum_{j=0}^{P}\sum_{k=0}^{P} \lambda_k \tilde{w}_j \frac{\langle \Psi_k \Psi_j \Psi_i \rangle}{\langle \Psi_i^2 \rangle} \tag{18}$$

This construction allows for a general representation using a new pseudospectral "overloaded" multiplication operation

$$w = \lambda * u * v \tag{19}$$

where each deterministic multiplication is transformed into a corresponding product of polynomial chaos expansions. This has great potential for automatic transformation of legacy deterministic code into the requisite stochastic PC code. Using this method, we can define other operators. For example, a pseudospectral inverse function:

$$w = \frac{1}{u} \approx \tilde{w} = 1 \oslash u = \sum_{a=0}^{P} \left[\frac{\left\langle \frac{1}{\sum_{k=0}^{P} u_k \Psi_k} \Psi_a \right\rangle}{\langle \Psi_a \Psi_a \rangle} \right] \Psi_a = \sum_{a=0}^{P} w_a \Psi_a \tag{20}$$

Note that the evaluation of the resulting pseudo-spectral mode strengths is straightforward for polynomial functions, $w(u)$, by addition of pseudospectral products, but requires additional work for other functions, such as inverses, exponentials, logarithms, etc. Generally, if a good local polynomial approximation for any of these functions is found, at least in the $\pm 3\sigma(u)$ of u_0, then substitution of that polynomial in the above projection will give an approximation to the necessary w_a's. Taylor series expansions may be used towards this end, however, the resulting representation is not convergent in general. Alternatively, the expectations can be evaulated using sampling or quadrature, but the associated computational cost rises very quickly with increasing number of stochastic dimensions ξ. Alternate approaches have been outlined in [20, 24, 25]. Inverses, $w = 1/u$, can be most robustly handled using a linear-system solve for the modes of w (see also section 4.3.4). Moreover, a general integration approach was presented for handling any function $w(u)$ as long as its derivative dw/du is a rational function of u [25]. We have utilized these constructions to develop a a generalized library of routines for pseudospectral PC operations that multiplies, inverts, or otherwise algebraically transforms spectral variables.

3 Non-Intrusive UQ

In the present discussion, we investigate the propagation of uncertainty from the model parameters to simulation outputs in the context of low Mach number reacting flow modeling using non-intrusive UQ, with a focus on supercritical water oxidation (SCWO). Supercritical water oxidation has been identified as a novel means of treating a wide array of dilute aqueous wastes [26]. At the typical operating conditions of 450 to 600^{o}C and 250 to 280 bar, free-radical oxidation reactions proceed rapidly and completely. The design of the SCWO process requires the development of appropriate combustion chemistry models. Sources of parametric uncertainty in these models include experimentally-determined reaction rate constants, thermodynamic properties, and transport properties.

In general, the propagation of parametric uncertainty can be studied non-intrusively using Monte Carlo (MC) simulations, with appropriate choices of model parameters over their ranges of uncertainty. However, this approach does not readily provide information about the sensitivity of model outputs to specific parametric uncertainties. An alternative non-intrusive approach is discussed here, based on the spectral polynomial chaos stochastic description of uncertain parameters and field quantities. Given MC sampling of the stochastic parameters, the corresponding solutions of the deterministic system are evaluated and projected onto the PC basis to compute the spectral mode coefficients. These coefficients are then used to construct probability density functions (PDFs) of the solution, to infer sensitivity to various model parameters, and to highlight the dominant sources of uncertainty.

This non-intrusive spectral projection (NISP) approach, which is based on [11], has the advantage of being applicable to legacy codes, which are run with varying parameters to compute the statistics and spectral mode values. It is important to note that, while NISP does provide sensitivity information, it actually goes well beyond sensitivity analysis in that it propagates the full probablistic representation of the model inputs to the model outputs. Moreover, the NISP-evaluated dependencies are related to the specific uncertainty in a given parameter, while sensitivity analysis compares equal parametric perturbations. Further, depending on the chosen order of the PC expansion, NISP also provides higher-order sensitivity information. Higher-order effects are not lumped into a single coefficient, but are considered independently and in terms of parameter-parameter interactions.

Other UQ methods are available, and for certain problems may have efficiency advantages. The determinisitic equivalent modeling method (DEMM) [27], is a probabilistic collocation method that generates a PC expansion of model outputs for systems with well-behaved response functions. It limits sampling to a subset of the roots of the next-higher order polynomial chaoses, and may exhibit instability at higher orders. The stochastic response surface method (SRSM) [28] expands sampling by using regression to generate coefficients from a complete set of higher-order roots. Both of these methods give good agreement with Monte Carlo for the estimation of output PDFs, and also fit the probabalistic response function to a set of PC coefficients. However, it is not clear that limiting sampling to the partial or full set of polynomial roots can adequately sample the necessary range of stochastic space, particularly for systems with strongly non-Gaussian reponses.

In the present discussion we apply the NISP procedure to two model problems. The first is a homogeneous ignition, a problem where uncertainty propagation has been studied previously by Phenix *et al.* [27]. The deterministic solver used for modeling ignition uses DVODE [29] for stiff integration of the species equations under constant temperature and pressure conditions. The second is a steady one-dimensional (1-D) premixed hydrogen-oxygen freely-propagating flame at SCWO conditions, computed with the Chemkin PREMIX code [30,31]. In both instances, we examine the mean and statistics of the solution and evaluate the corresponding spectral PC-modes, given known uncertainties in reaction rate constants and thermodynamic properties of the model based on [27]. We arrive at broad measures of confidence in model predictions, focusing on detailed chemistry. We also identify dominant sources of uncertainty in computed species concentrations, and highlight specific model parameters where reduction of uncertainty via additional experimental measurements can most effectively improve confidence in model predictions.

3.1 NISP Formulation

The formulation and numerical implementations of the deterministic solvers used for both the ignition and 1-D flame problems are well documented in the literature [29–31]. We will focus instead on the description

of the NISP model.

As mentioned above, we focus on parametric uncertainty. As outlined in section 2.1, we represent each uncertain model parameter as a stochastic quantity with known probability density function (PDF). Thus a parameter λ is expressed using the PC expansion,

$$\lambda = \sum_{i=0}^{P} \lambda_i \Psi_i \tag{21}$$

where, the λ_i's are the known spectral mode strengths of λ.

$$\lambda_i = \frac{<\lambda \Psi_i>}{<\lambda_i^2>}, \quad i = 0, \ldots, P \tag{22}$$

Further, the model solution u is represented using the PC expansion, according to:

$$u(x,t) = \sum_{k=0}^{P} u_k(x,t) \Psi_k \tag{23}$$

where the u_k's are the *unknown* spectral modes of u, given by

$$u_k = \frac{\langle u \Psi_k \rangle}{\langle \Psi_k^2 \rangle}, \quad k = 0, \ldots, P \tag{24}$$

The NISP approach uses realizations of the computed deterministic solution to evaluate the expectations in Eq. 24, thereby reconstructing the PC expansion of u. This procedure involves the following steps :

1. Define PDFs for the model parameters, using known distributions or assuming normal, lognormal, or other general forms.
2. Determine the corresponding spectral PC expansion for each of the parameters.
3. Sample the vector of gaussians $\theta = \{\xi_1, \xi_2, \cdots, \xi_N\}$, and use it to evaluate Ψ_k, $k = 0, \ldots, P$ and the corresponding parametric realizations for the vector of parameters $\{\lambda_1, \lambda_2, \cdots, \lambda_N\}$, given the parameter PC expansions.
4. For each realization of the vector of parameters, solve the deterministic problem, and compute the corresponding realization of the solution u.
5. Evaluate the above expectations specified in Eq. 24, over a sufficiently large number of samples, and find the spectral coefficients u_k of the solution. Thus, for M realizations, the modes are found by

$$u_k = \frac{\sum_{m=1}^{M} (u)_m (\Psi_k)_m}{\sum_{m=1}^{M} [(\Psi_k)_m]^2}, \quad k = 0, \ldots, P \tag{25}$$

where $()_m$ denotes the m-th realization.

In this study, the above NISP analysis of simulation results is performed using the DAKOTA toolkit [32,33] using Latin-Hypercube sampling [22] (LHS) for normal random variables. Convergence of the sampling is tracked by examining the maximum standard deviation, calculated directly from the evolving PC expansion. Each LH sample provides a vector of normal random variables ξ_i. These are used to sample from lognormal distributions of the Arrhenius pre-exponential rate constants for the forward reaction rates k_f, and Gaussian distributions of the enthalpies of formation ΔH_f^o of the species. The reverse reaction rates are related to the inverse equilibrium constant, which is also log-normally distributed due to its exponential dependence on the Gibbs free energies and therefore the enthalpies of formation [27].

In terms of computational cost, Monte Carlo methods, by design, require many iterations. For the 0-D ignition chemistry, we could perform approximately 125 realizations per hour on a single-processor Pentium

III workstation. For 1-D flames, using the existing Chemkin PREMIX codes, 20 realizations per hour could be expected. For typical runs of 10,000-30,000 samples, this clearly requires considerable computing time. However, the non-intrusive nature of the method described above lends itself to simple parallel distribution of the computing load. Individual machines can process a subset of the samples, using a consistent set of sampling points, and the actual statistics can be compiled through post-processing. The use of multiple independent machines allowed the most intensive calculations to be performed within a reasonable timeframe.

Analysis of the results uses the spectral modes to infer both uncertainty and sensitivity information. To first order in ξ, neglecting second and higher-order terms, we have

$$\frac{\partial u}{\partial \xi_k} = u_k \tag{26}$$

such that the amplitude and sign of a spectral mode is a measure of the influence of the associated parameter on the solution. Note that this sensitivity information includes the full non-linear coupling of associated species and temperature variations in the system. When comparing flame solutions resulting from different values of the Arrhenius rate constant A_k, the net change in the rate of progress of reaction k is not simply due to the change in A_k, but also due to the associated changes in all species concentrations and temperature. These effects can be quite significant as will be observed below.

3.2 NISP Results and Discussion

3.2.1 0-D integration of the chemistry

In the previous study by Phenix *et al* [27], the DEMM was used with Monte Carlo to propagate uncertainty in supercritical-water oxidation. Using sensitivity analysis, the study developed a reduced variant of the hydrogen oxidation mechanism of Yetter [34] that had proven useful in earlier SCWO modeling studies [35]. This mechanism is given in Table 1. To account for experimental uncertainty, uncertainty in the adaptation of the mechanism to SCWO conditions, and limited stable-species mixture data in supercritical water, each forward rate constant, k_f, was represented by a log-normal probability distribution. The distributions were parameterized via a median value and a multiplicative uncertainty factor, S, giving upper and lower bounds for each $k_{f,j}$:

$$\text{Median}(k_{f,j}) \times S \tag{27}$$

$$\text{Median}(k_{f,j}) \div S \tag{28}$$

Uncertainty factors used in this analysis and the Phenix study are listed in Table 1. The standard-state enthalpies of formation were modeled as Gaussian distributions, with mean values and standard deviations given in Table 2.

Reaction			A	n	E_a/R	S
1. OH + H	$\leftrightarrow$	H_2O	1.620E+14	0	75	3.16
2. H_2 + OH	$\leftrightarrow$	H_2O + H	1.024E+08	1.6	1660	1.26
3. H + O_2	$\leftrightarrow$	HO_2	1.481E+12	0.6	0	1.58
4. HO_2 + HO_2	$\leftrightarrow$	H_2O_2 + O_2	1.867E+12	0	775	1.41
5. H_2O_2 + OH	$\leftrightarrow$	H_2O + HO_2	7.829E+12	0	670	1.58
6. H_2O_2 + H	$\leftrightarrow$	HO_2 + H_2	1.686E+12	0	1890	2.00
7. H_2O_2	$\leftrightarrow$	OH + OH	3.000E+14	0	24400	3.16
8. OH + HO_2	$\leftrightarrow$	H_2O + O_2	2.891E+13	0	-250	3.16

Table 1: Reduced hydrogen oxidation mechanism with estimated multiplicative uncertainty factors [27]. $k = AT^n \exp(-E_a/RT)$ with units of cm^3, mol, s, and K.

Species	μ_0	2σ
H	52.10	0.01 kcal/mol
OH	9.3	0.02
H_2O	-57.80	0.01
H_2O_2	-32.53	0.07
HO_2	3.0	0.5

Table: 2 Mean values and standard deviations of the species standard-state heats of formation ΔH_f^o [27].

In the DEMM analysis, the response functions were represented as PDFs to estimate the effect of uncertain input parameters. Our NISP analysis also represents the responses in terms of PDFs, but with greatly enhanced sampling of phase space. Since DEMM selects collocation points only from the roots of the next higher Hermite polynomial, it is not clear that such limited sampling will be effective for all systems, particularly those with larger high-order dependencies. Our analysis also uses the coefficients of the polynomial chaos expansion to characterize the detailed dependencies of each response on each uncertain input parameter.

For this study, we repeated the analysis using NISP techniques and second-order PC expansions. Using the DVODE solver, we integrated the ODE system over a 10s time interval. The vector of random variables ξ_i was used to sample from the reaction rate and enthalpy distributions for 30,000 independent realizations. Each set of sampled parameters was used to integrate the species conservation equations and to generate profiles of concentration vs. time for each species. The mean and standard deviation for each species concentration was computed, and the concentration profiles were projected onto the PC basis to calculate the deterministic coefficients, $u_k(j,t)$, as functions of species j and time t. The system was integrated at constant T=823 K and P=246 bar, with initial concentrations of $c_{H_2} = 0.481 \times 10^{-3}$mol/cm^3, $c_{O_2} = 0.243 \times 10^{-3}$mol/cm^3, and $c_{H_2O} = 0.999$mol/cm^3. While it is also possible to integrate the system with stochastic initial conditions, the present study focuses on uncertainty in reaction rate pre-exponential factors and enthalpies of formation. As such, the statistics and PC mode values evaluated herein necessarily correspond to the above deterministic initial conditions. In the following, spectral mode numbering proceeds from 1 to 8 by reaction number for the pre-exponential rate constants in Table 1, and from 9 to 13 for species H, OH, H_2O, H_2O_2, HO_2 respectively for the enthalpies of formation in Table 2. Species H_2 and O_2 have identically zero enthalpies of formation.

Figure 1 shows the evolution of OH radical concentration (c_{OH}) vs. time for the reduced chemical system. Upper and lower bounds designate $c_{OH} \pm \sigma$ as calculated directly from the MC statistics during the NISP production run. This profile outlines the total uncertainty generated by the estimated parametric uncertainty, with 2σ approaching the magnitude of the mean. The results of Phenix *et al* showed similar levels of uncertainty for various species, with variations of 70 to 180% from median concentrations. The standard deviation can also be calculated directly from the existing PC coefficients by the summation:

$$\sigma^2 = \sum_{k=1}^{P} u_k^2 < \Psi_k^2 > \tag{29}$$

which produces a similar numerical result for standard deviation as the direct evaluation from the MC statistics. For our system with 13 uncertain parameters (eight reaction pre-exponentials and five enthalpies of formation) and second-order PC expansions, $P = 105$ modes.

The time-evolution of the first-order ($\Psi_k = \xi_k$) spectral modes in the PC-expansion for c_{OH} is shown in Figure 2. These modes correspond to uncertainties in the Arrhenius pre-exponential terms A_k of the forward reaction rates $k_{f,k}$. It is evident that uncertainties in the pre-exponential rate constants of reactions 5, 7, and 8 dominate the expansion and therefore dominate the generation of the total uncertainty in c_{OH}. This is consistent with the results of Phenix *et al*, who identified Rn.7 as dominant for the 0-D evolution of the H_2 consumption, although the study did not directly address uncertainty in the concentrations of intermediates. We find Rn.7 to be the dominant OH production channel during the ignition process, while Rn.2 is the dominant OH consumption channel. An increase in A_7 might then be expected to increase OH production and therefore OH concentration, which is indeed observed in Fig. 2 and in the time evolution of c_{OH}. As for Rn.5, its net progress at the unperturbed parameter values is in the reverse direction, thus producing OH,

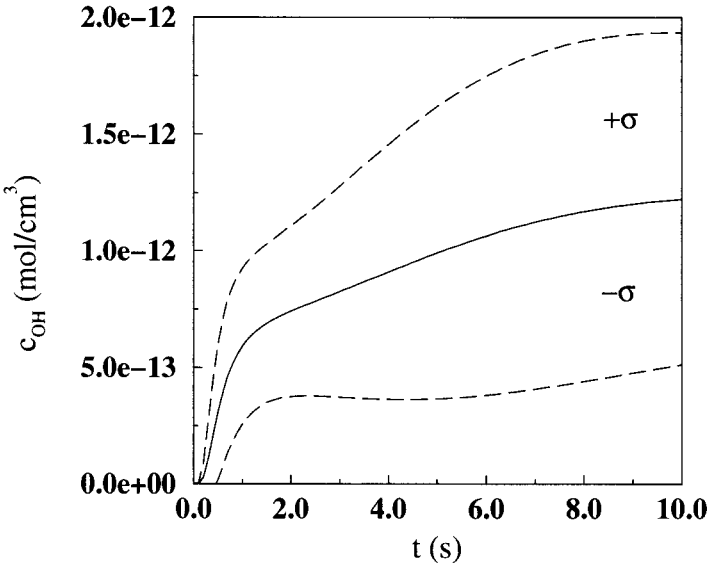

Figure 1: OH concentration vs. time for 0-D integration of chemistry, with $\pm\sigma$ bounds.

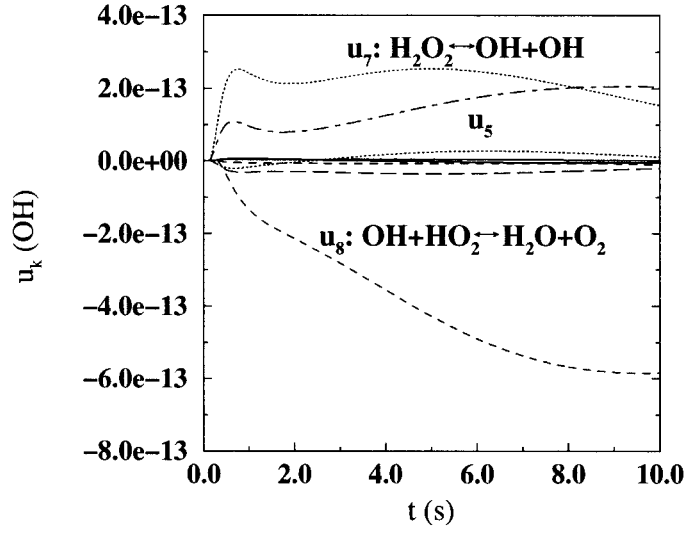

Figure 2: Spectral decomposition of OH concentration profile, with modes 5, 7, and 8 representing first-order dependence on forward reaction rates.

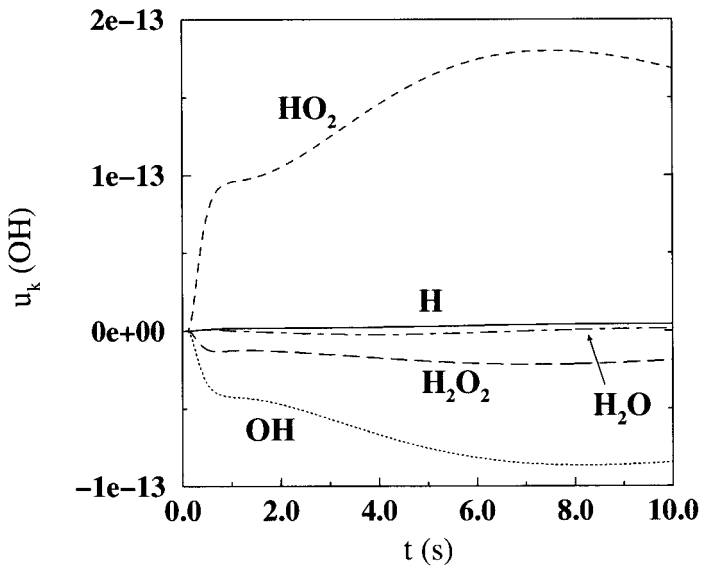

Figure 3: Spectral decomposition of OH concentration profile for modes 9 through 13, representing first-order dependence on heats of formation.

albeit at a relatively small rate. Thus, an increase in A_5 might be expected to lead to an increase in the forward rate of Rn.5, lower OH production and less OH. In fact, we find that increasing A_5, and the associated changes in species production rates and concentrations, leads to stronger net forward rates of Rns. 2,3,4 and 7 in the first 1/2-ms of the ignition process. This leads to a faster OH production rate at early time, and increased overall OH concentration, which is shown by the indicated evolution of u_5 in Fig. 2. Note that the net effect on the rate of progress of Rn.5 is a stronger *reversal*, contributing to the increased rate of OH production. In a similar way, the negative influence of u_8 can be explained based on the overall resultant changes to the reaction network at the larger/smaller A_8.

It is noteworthy that uncertainties in parameters of Rns. 5 and 8, both somewhat insignificant OH channels, have such a significant impact on the system and lead to large contributions to the total uncertainty in OH prediction. By propagating actual uncertainty values, rather than simply perturbing parameters to gage sensitivity, we can see how both the influence of a given reaction and the uncertainties associated with reaction rates combine to create a net uncertainty in simulation results. The spectral decomposition not only shows sensitivity information, but also indicates where a given uncertain parameter holds the most influence. In Fig. 2, Rn.7 provides the greatest contribution to uncertainty at $t < 1$ s, with Rn.8 dominating at longer times. Furthermore, the relative dependence of Rns.5 and 7, and consequently their relative contribution to uncertainty propagation, changes with time as the concentration of OH increases.

Figure 3 gives mode strengths for u_9 through u_{13}, which represent the first-order variation of $c_{\mathrm{OH}}(t)$ due to uncertainty in the standard-state enthalpies of formation. The importance of $\Delta H^o_{f,\mathrm{HO_2}}$ to the total uncertainty is highlighted, in agreement with the observations of Phenix *et al.* We also see a significant negative dependence on $\Delta H^o_{f,\mathrm{OH}}$, a parameter on which the equilibrium for Rns.1, 2, 5, 7, and 8 depend.

For 13 stochastic dimensions and a second-order expansion, a total of 105 modes are present in the PC expansion. In this study, the second-order modes u_{14} to u_{105}, reflecting both higher-order dependence on specific parameters as well as coupling between parameters, are approximately an order of magnitude smaller than first-order mode ($< 2.0 \times 10^{-14}$). However, the large number of these modes makes their aggregate contribution to the uncertainty quite significant (up to 50%). Also, for systems with strongly non-Gaussian response behavior, higher-order expansions may become necessary to represent skewed or highly-asymmetrical PDFs. For this particular problem, it is fortuitous that the response functions are well-behaved and can be accurately represented as moderately-skewed Gaussians using second-order PC expansions. This will certainly not be the case for many systems of interest, therefore higher-order analysis and more extensive sampling would be

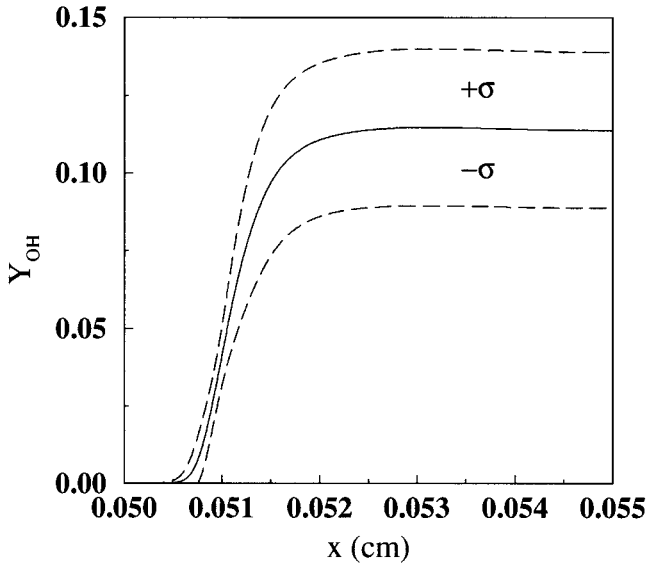

Figure 4: Profile of OH mass fraction vs. position in a 1-D premixed supercritical-water flame, with $\pm\sigma$ bounds.

required. NISP allows an arbitrarily high order and large number of samples as computation resources allow.

3.2.2 1-D premixed flame simulations

We next extend the NISP technique to the analysis of a 1-D hydrogen flame. We use as our model the Chemkin PREMIX package with SCWO inlet conditions at T=823K, P=246 bar and a stoichometric fuel mixture. The MC integration uses 22,000 samples from the log-normal and Gaussian distributions for the eight reaction rates and five enthalpies of formation to generate PREMIX input parameters. Convergence was measured by tracking the maximum standard deviation computed directly from the evolving PC expansion. Each flame was normalized to a standard x-coordinate system by matching the point at which the concentration of H_2 has reached 10% of total consumption.

In Fig. 4, the mass fraction of OH, $Y_{\mathrm{OH}}(x)$, is plotted vs. position. Upper and lower bounds of Y_{OH}, $Y_{\mathrm{OH}}(x) \pm \sigma$ are given, calculated directly from the PC expansion. The uncertainty due to the model parameters grows over x, with peak values occurring inside the primary flame reaction zone (x=0.0505 cm to 0.0515 cm). Profiles of the other intermediates and products–HO_2, H_2O_2, and H_2O–also show similar localized increases of total uncertainty.

Figure 5 highlights the four largest first-order modes of Y_{OH} from the spectral decomposition. It is clear that Rn.5 dominates the accumulation of uncertainty within the primary flame. In this case, u_7 is relatively insignificant (< 0.0002) over all x. The selected modes show how changes in $k_{f,j}$ control the shape of the mass fraction profile of OH. The change in the sign of u_1, u_5, and u_8 near $x = 0.051$ cm corresponds to the inflection point in the $Y_{\mathrm{OH}}(x)$ profile, and highlights the effect of variation in the respective reaction rates on the local slope of the OH profile. Further, the modes describe where, and to what degree, a specific parameter contributes to the total uncertainty in Y_{OH}. Reaction flux analysis (not shown) indicates that Rn.7 dominates OH production in this flame, with a smaller contribution by Rn.5 (net rate in the reverse direction). On the other hand, Rn.2 is the main OH consumer, with lesser contributions by Rns.1 and 8.

Let us consider the significance of the variation in u_5 in the figure, corresponding to the effect of changes in the pre-exponential Arrhenius term A_5. Comparison of flame structure between the mean and higher values of A_5 indicates that the slope of the OH profile increases with increased A_5. The change in the sign of u_5 is a reflection of the difference between the mean OH profile and the higher-slope OH profile. The increase in slope is driven by an increase in the net OH production and consumption rates (not shown), as a result of changes in the rates of *all* the OH reactions towards higher production/consumption. In particular,

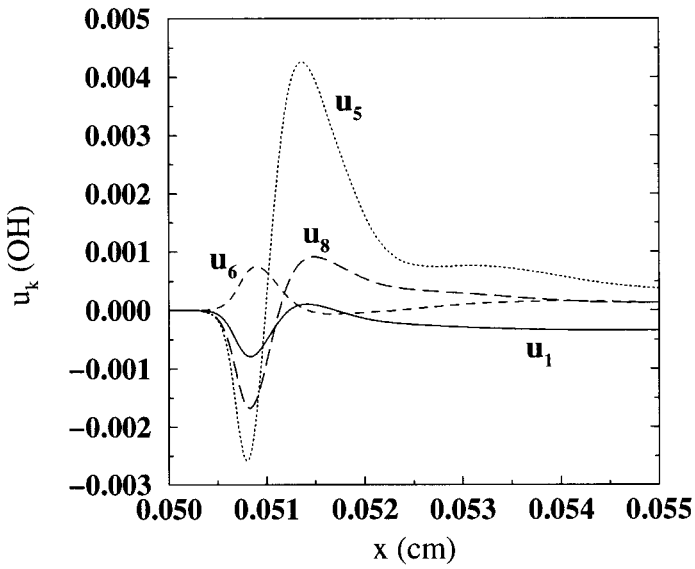

Figure 5: Spectral decomposition of the mass fraction of OH, highlighting first-order dependence on reactions 1, 5, 6, and 8.

Rn.5 is found to have a larger net *reverse* rate at the higher A_5, again reflecting the coupling of changes in all species and temperature associated with the single change in A_5. Here again, we note the significance of a relatively minor production/consumption channel on the overall uncertainty in the predicted species concentration profile despite a comparatively low S.

Figure 6 describes the first-order dependence of Y_{OH} on the enthalpies of formation. Here, $\Delta H^o_{f,OH}$ shows the greatest significance, with lesser contributions to the overall uncertainty in OH by the enthalpies of formation of H_2O, HO_2 and H_2O_2. As with the 0-D analysis, the $\Delta H^o_{f,j}$ dependencies reflect the roles of the enthalpies of formation in the reaction equilibria, indicating the net sensitivity of the reaction network to particular thermodynamic parameters, and the importance of each parameter in uncertainty propagation. All second-order modes were an order of magnitude smaller, and are not shown.

The analysis is repeated for the H_2O_2 intermediate in Figures 7–9. For this intermediate, in Fig. 7 we see that the uncertainty in the H_2O_2 mass fraction varies greatly with position, with a maximum uncertainty inside the 1-D flame from x=0.0500 cm to 0.0505 cm, little uncertainty near x=0.05075 cm, and a small, slowly increasing, and eventually constant degree of uncertainty downstream. Tracking the individual realizations of $Y_{H_2O_2}$, we find that, for any set of parameters, the mass fraction passes near zero near x=0.05075 cm, resulting in minimum total uncertainty at that point. This uncertainty minimum separates two distinct flame regions, such that the relatively small uncertainty in the post-flame H_2O_2 mass fraction is effectively independent of the larger uncertainty in the primary flame region. Note specifically the *large* uncertainty in H_2O_2 mass fraction within the primary flame, where the standard deviation is larger than the mean. The large range of values of $Y_{H_2O_2}$ spanned by the data suggests that the reduced chemical model may lack robustness for predicting this species, given existing uncertainties in chemical and thermodynamic parameters. Reducing the parametric uncertainty in the reaction rates, particularly Rn. 5, would reduce the total accumulation of uncertainty in $Y_{H_2O_2}$ and enhance the robustness of the model.

In order to identify the causes behind this observed uncertainty in $Y_{H_2O_2}$, we plot the associated first-order spectral modes in Figure 8. Here, u_5 again dominates, reaching twice the magnitude of u_7 or u_8. The decay of all spectral modes to near zero in the vicinity of x=0.05075 cm reflects the above observed minimum in uncertainty at this location. Note that the main production and consumption zones of H_2O_2 in the deterministic/unperturbed flame are to the left of the minimum at x=0.05075 cm, with Rns.4 and 5 being the dominant production channels, and Rn.7 the dominant consumption channel. The effect of A_5-uncertainty can again be studied by comparing the flame structure at the mean and high A_5 values. Increasing A_5 leads to

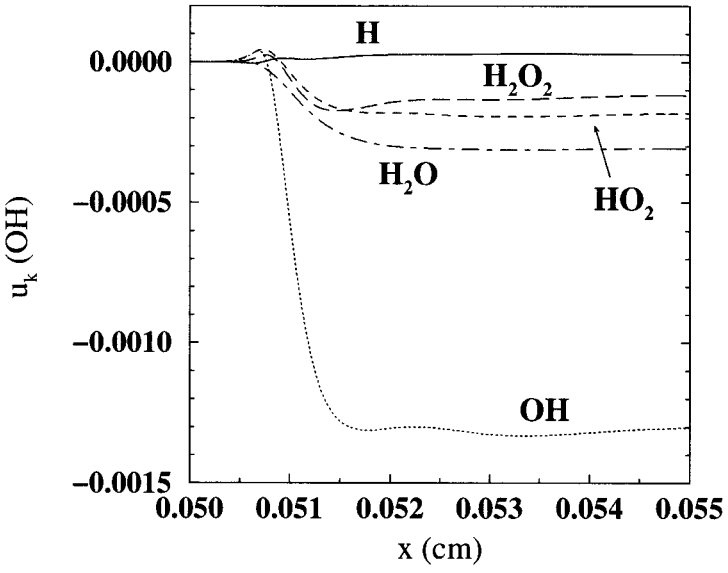

Figure 6: Spectral decomposition of the OH mass fraction, highlighting the first-order dependence on heats of formation.

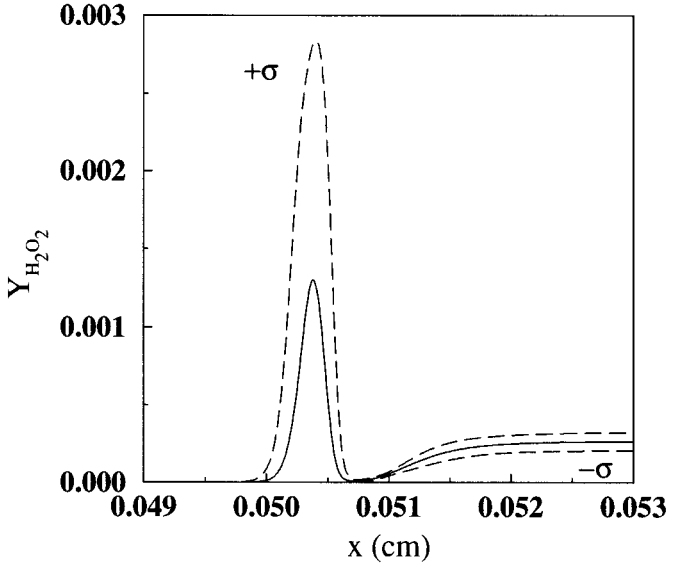

Figure 7: Profile of H_2O_2 mass fraction vs. position in a 1-D premixed supercritical-water flame, with $\pm\sigma$ bounds.

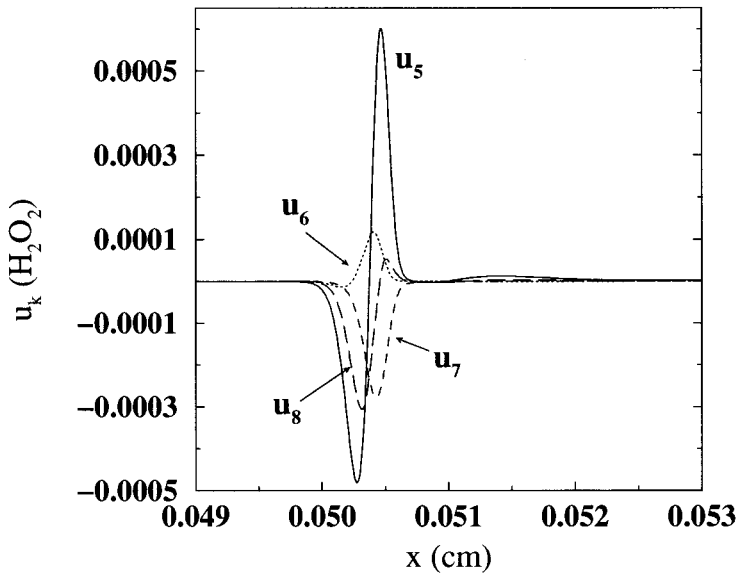

Figure 8: Spectral decomposition of the H_2O_2 mass fraction, highlighting the first-order dependence on reactions 5, 6, 7, and 8.

an increase in both production and consumption peaks of H_2O_2 (not shown). These are driven by changes in all reaction rates of progress resulting from the change in A_5 and associated change in species concentration and temperature. Particularly significant increases in the production rate of H_2O_2 at $x < 0.05075$ are due to Rns.4 and 5 (Rn.5 again going in a net reverse direction). A significant increase in consumption of H_2O_2 in this region is due to an increase in the net reverse rate of Rn.7. All of these changes are driven by the increase in A_5 and the associated changes in flame structure. The net result is an increased peak value and smaller width of the $Y_{H_2O_2}$ profile–hence larger slopes that, as with OH, create the associated signature observed in the u_5 profile in Fig. 8. Note that u_5 is also the significant source of H_2O_2 uncertainty downstream, as seen in Fig. 8.

The first-order enthalpy-of-formation spectral modes of $Y_{H_2O_2}$ are shown in Fig. 9. Uncertainty in the enthalpy of formation of OH is again significant, as well as that of HO_2. On the other hand, these amplitudes are small compared to those resulting from the uncertainties in rate constants, in Fig. 8, and therefore have lesser impact on the robustness of the chemical model.

A similar analysis performed for other species reveals that A_5 and $\Delta H^o_{f,OH}$ are the dominant parameters for all species mass fraction profiles in this mechanism. Clearly, a reduction of the experimental uncertainty in both of these quantities (as well as in $\Delta H^o_{f,HO_2}$) will have a large impact towards improving robustness of the chemical SCWO model and increasing confidence in model predictions.

One feature that can be discerned through a spectral analysis of uncertainty is not only to what degree, but where and when do particular paramteric uncertainties manifest themselves. In Fig. 2 and Fig. 3, we see that a parameter's contribution to total uncertainty can vary with time or flame position and that different parameters propagate uncertainty in different chemical regimes. Fig. 10 separates the chemical and thermodynamic effects of uncertainty propagation into Y_{OH} in terms of contribution to the standard deviation. Shown are the partial standard deviations computed directly from selected modes of the PC expansion using Eq. 29. The uncertainty contributed through chemical reaction pre-exponential uncertainties can be seen in the shaded curves, with combinations of Rns. 1 and 6, Rns. 1, 6, and 8, and Rns. 1, 6, 8, and 5 highlighted. The dotted line gives the total contribution due to all 1st-order modes u_1-u_{13}. It is clear that chemical uncertainties dominate propagation in the flame front, while the remaining thermodynamic parameters become increasingly important in the products side of the flame as the products approach equilibrium downstream of the flame.

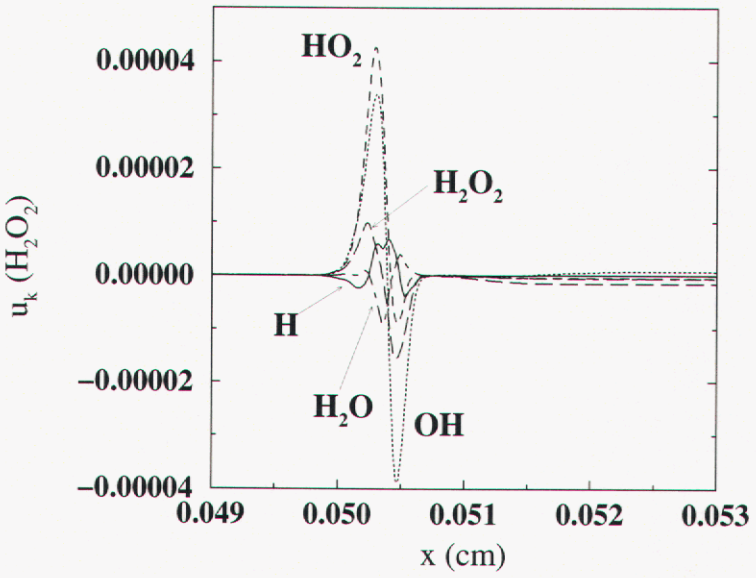

Figure 9: Spectral decomposition of the H_2O_2 mass fraction, highlighting the first-order dependence on heats of formation.

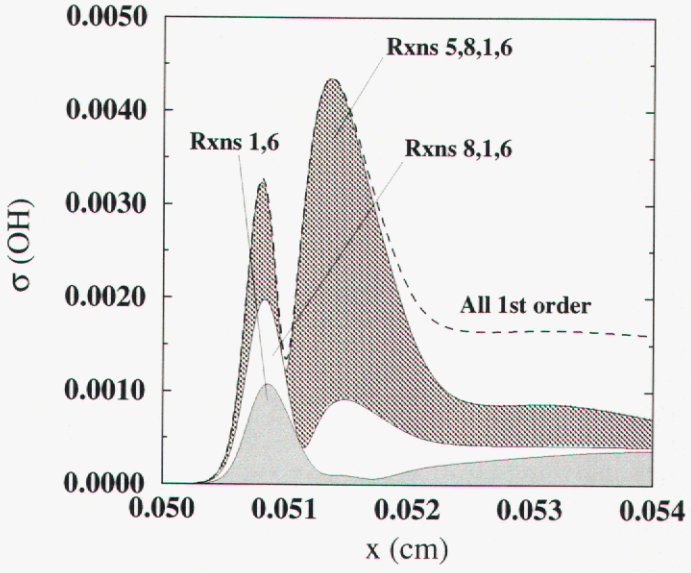

Figure 10: Standard deviation of OH mass fraction, showing the cumulative contribution of first-order dependencies on selected reactions and the total first-order contribution (reactions and enthalpies).

3.3 Non-Intrusive UQ Summary

A generalized, non-intrusive spectral projection scheme has been implemented to propagate parametric uncertainty in reacting-flow simulations. Compared to global Monte-Carlo estimation of total uncertainty, spectral methods quantify the source of the uncertainty, the propagation of uncertainty through the model, and the sensitivity of model outputs to specific parameters.

For homogeneous ignition chemistry, NISP provides sensitivity information that is consistent with previous work. Quantification of spectral modes adds an additional level of understanding, identifying the significance of individual uncertain parameters and determining where within the evolution of the system each parameter has influence. Extending the analysis to a simple 1-D problem allows the analysis of uncertainty propagation in different regions of a premixed flame, identifying relationships between parameters, specific flame features, and the total propagation of uncertainty.

The consequences of such an analysis are significant. The dramatic amplification of parametric uncertainty within a particular chemical model may call into question the robustness of the model. Further, highlighting the parameters primarily responsible for the large uncertainty in model outputs is a valuable indicator of where additional experimental measurements may best be targeted. In the particular SCWO system at hand, parameters that merit further measurements are the rate of Rn.5 and the enthalpies of formation of OH and HO_2, as well as the rates of Rns. 7 and 8. Better estimates of these parameters should improve the overall ability of the model to represent the system being studied.

In comparison to the DEMM and SRSM method used before, this method provides similar stochastic information while making fewer assumptions about the system response. For systems with simple, Gaussian-like reponses, convergence should be quick and efficient. For more complex systems, particularly chemical systems subject to the positive-concentration constraint, $c_i >= 0.0$, higher-order terms are likely to be significant for intermediates or during the early stages of an ignition problem. Unphysical PDFs (distributions with significant probabilities for negative concentrations) or non-convergent expansions (PC coefficients increasing with increasing order) would indicate that the selected order is not sufficent to represent the system response.

Finally, this analysis is readily extendable to multiple dimensions and greater numbers of uncertain parameters, while preserving the integrity of the realization engine through the non-intrusive construction. However, the computational cost associated with monte-carlo sampling can render the intrusive UQ analysis impractical. In many applications, it is simply not possible to compute many thousands of realizations, even on massivelly parallel computational hardware. Alternative "sampling" techniques based on quadrature [24] and cubature/sparse-quadrature methods can be useful in this regard. The intrusive UQ approach provides another potential means of addressing this difficulty. This is the subject of the following section.

4 Intrusive UQ

This section addresses intrusive UQ in chemical systems by developing the formulation for a pseudo-spectral chemical source term for detailed chemical mechanisms with multiple parametric uncertainties in rate constants and thermodynamic properties. Further, we address the numerical challenges inherent in such a construction for highly-nonlinear chemical systems. The application focus is on 0-D homogeneous ignition, a problem that highlights the utility and potential challenges of this approach. The treatment starts with a description of the components of the intrusive PC formulation for a generalized chemical source term. We then use these tools to examine homegeneous ignition for a detailed reaction mechanism, the advantages and disadvantages of intrusively-reformulated models, and issues of stability and the limits of the formulation.

4.1 Chemical source term

4.1.1 Definition of the chemical system

A key to the construction of a spectral reacting-flow code is an efficient stochastic chemical source term. In the following, we present dimensionless deterministic and stochastic formulations for a chemical source term.

Consider a spatially homogeneous perfect gas mixture of N species χ_i, with $i = 1,\ldots,N$, participating in

M reactions:

$$\sum_{i=1}^{N} \nu'_{ik} \chi_i \iff \sum_{i=1}^{N} \nu''_{ik} \chi_i, \quad k = 1, \ldots, M \tag{30}$$

where ν'_{ik} and ν''_{ik} are the stoichiometric coefficients for species i appearing as a reactant or product, respectively, in reaction k. Given this set of reactions, the mass production rate of species i is given by

$$w_i = W_i \sum_{k=1}^{M} \nu_{ik} C_k \mathcal{R}_k \tag{31}$$

where W_i is the molar mass of species i,

$$\nu_{ik} = \nu''_{ik} - \nu'_{ik} \tag{32}$$

and, C_k is a correction factor due to third-body and/or pressure-fall-off corrections [30]. This factor is given by

$$C_k = \begin{cases} 1 & \text{for a non-third-body, non-pressure-fall-off rxn} \\ \zeta_k = \sum_{i=1}^{N} \beta_{ik} c_i & \text{for a third-body, non-pressure-fall-off rxn} \\ \left(\frac{P_r^k}{P_r^k + 1}\right) F_k & \text{for a pressure-fall-off rxn (third body or not)} \end{cases} \tag{33}$$

where, β_{ik} is the third-body efficiency of species i in reaction k, P_r^k is given by

$$P_r^k = \begin{cases} \dfrac{k_k^{F,0} c_M}{k_k^{F,\infty}} & \text{for a pressure-fall-off third-body (+M) rxn} \\ \dfrac{k_k^{F,0} c_i}{k_k^{F,\infty}} & \text{for a pressure-fall-off non-third-body (+}\chi_i\text{) rxn} \end{cases} \tag{34}$$

Here, c_M is the total concentration of the mixture, $k_k^{F,0}$ and $k_k^{F,\infty}$ are the low and high pressure forward rates of reaction k, respectively [30], and F_k is a known function of P_r^k and T describing fall-off behavior for each pressure fall-off reaction k [30]. Further, $\mathcal{R}_k$ is the rate of progress of reaction k, given by

$$\mathcal{R}_k = k_k^F \prod_{i=1}^{N} c_i^{\nu'_{ik}} - k_k^R \prod_{i=1}^{N} c_i^{\nu''_{ik}} \tag{35}$$

where k_k^F and k_k^R are the forward and reverse rates of reaction k, $c_i = \rho Y_i / W_i$ is the molar concentration of species i, ρ is the mass-density of the mixture, and Y_i is the mass fraction of species i in the mixture.

The time-evolution of the chemical system is governed by the ODE system,

$$\frac{dc_i}{dt} = \frac{\mathrm{Da}}{W_i} w_i, \quad i = 1, \ldots, N-1 \tag{36}$$

$$\frac{d\rho}{dt} = \frac{\mathrm{Da}}{c_p T} \sum_{i=1}^{N} h_i w_i - \mathrm{Da} \overline{W} \sum_{i=1}^{N} \frac{w_i}{W_i} \tag{37}$$

with algebraic constraints resulting from mass conservation,

$$\sum_{i=1}^{N} Y_i = 1 \tag{38}$$

and the perfect gas state equation:

$$P_0 = \frac{\rho T}{\overline{W}} \tag{39}$$

In this nomenclature [36], Da is the Damköhler number defined based on reference quantities, T is the temperature, c_p is the mixture specific heat at constant pressure, h_i is the specific enthalpy of species i, P_0 is the stagnation pressure (assumed constant), $\overline{W} = 1/\sum_{i=1}^{N} Y_i W_i$ is the molar mass of the mixture. These equations are closed with initial conditions $c_i(t=0) = c_i^0$ and $\rho(t=0) = \rho^0$.

4.1.2 Fully spectral construction

We illustrate in this section the necessary spectral construction for the representation of the reaction rates of progress $\mathcal{R}_k$ given above in 35, assuming known spectral expansions for the forward and reverse rates, and the concentrations. Moreover, we illustrate this for brevity using only the forward term, given that the extension to the reverse term is straightforward in this context. Thus, we seek to present the full spectral construction for $\mathcal{R}_k^F$, given by

$$\mathcal{R}_k^F = k_k^F \prod_{i=1}^{N} c_i^{\nu'_{ik}}. \tag{40}$$

To begin with, in order to exclude zero exponents, define the set of species indices containing those species with non-zero stoichiometric coefficients on the reactants side of reaction k. This set is given by,

$$I_k = \{i | \nu'_{ik} \neq 0\} = \{i_1^k, i_2^k, \ldots, i_{L_k}^k\} \tag{41}$$

and, dropping the k-sub/super-scripts for clarity, we have the set

$$I = \{i_1, i_2, \ldots, i_L\} \tag{42}$$

such that, again dropping the k's,

$$\mathcal{R}^F = k^F \prod_{p=1}^{L} c_{i_p}^{\nu'_{i_p}} = k^F \prod_{p=1}^{L} \left(\sum_{j=0}^{P} (c_{i_p})_j \Psi_j \right)^{\nu'_{i_p}} \tag{43}$$

Next, we have by inspection, for integer $n > 0$,

$$\left(\sum_{j=0}^{P} a_j \right)^n = \sum_{j_1=0}^{P} \sum_{j_2=0}^{P} \cdots \sum_{j_n=0}^{P} a_{j_1} a_{j_2} \cdots a_{j_n} = \sum_{j_b=0}^{P} \Bigg|_{b=1}^{n} \prod_{q=1}^{n} a_{j_q} \tag{44}$$

where

$$\sum_{j_b=0}^{P} \Bigg|_{b=1}^{n} \equiv \sum_{j_1=0}^{P} \sum_{j_2=0}^{P} \cdots \sum_{j_n=0}^{P} \tag{45}$$

such that

$$\mathcal{R}^F = k^F \prod_{p=1}^{L} \sum_{j_b=0}^{P} \Bigg|_{b=1}^{\nu'_{i_p}} \prod_{q=1}^{\nu'_{i_p}} (c_{i_p})_{j_q} \Psi_{j_q}. \tag{46}$$

Further,

$$\begin{aligned} \mathcal{R}^F &= k^F \left(\sum_{(j_b)_1=0}^{P} \Bigg|_{b=1}^{\nu'_{i_1}} \prod_{q=1}^{\nu'_{i_1}} (c_{i_1})_{(j_q)_1} \Psi_{(j_q)_1} \right) \left(\sum_{(j_b)_2=0}^{P} \Bigg|_{b=1}^{\nu'_{i_2}} \prod_{q=1}^{\nu'_{i_2}} (c_{i_2})_{(j_q)_2} \Psi_{(j_q)_2} \right) \cdots \\ &\quad \cdots \left(\sum_{(j_b)_L=0}^{P} \Bigg|_{b=1}^{\nu'_{i_L}} \prod_{q=1}^{\nu'_{i_L}} (c_{i_L})_{(j_q)_L} \Psi_{(j_q)_L} \right) \\ &= \sum_{(j_b)_1=0}^{P} \Bigg|_{b=1}^{\nu'_{i_1}} \sum_{(j_b)_2=0}^{P} \Bigg|_{b=1}^{\nu'_{i_2}} \cdots \sum_{(j_b)_L=0}^{P} \Bigg|_{b=1}^{\nu'_{i_L}} \prod_{p=1}^{L} \prod_{q=1}^{\nu'_{i_p}} (c_{i_p})_{(j_q)_p} \Psi_{(j_q)_p} \end{aligned} \tag{47}$$

or,

$$\mathcal{R}^F = k^F \sum_{(j_b)_z=0}^{P} \Bigg|_{b=1}^{\nu'_{i_z}} \Bigg|_{z=1}^{L} \left(\prod_{p=1}^{L} \prod_{q=1}^{\nu'_{i_p}} (c_{i_p})_{(j_q)_p} \right) \left(\prod_{p=1}^{L} \prod_{q=1}^{\nu'_{i_p}} \Psi_{(j_q)_p} \right) \tag{48}$$

Finally, with

$$k^F = \sum_{i=0}^{P} k_i^F \Psi_i \tag{49}$$

we have

$$\mathcal{R}^F = \sum_{i=0}^{P} \sum_{(j_b)_z=0}^{P} \left|_{b=1}^{\nu'_{iz}} \right|_{z=1}^{L} \left(k_i^F \prod_{p=1}^{L} \prod_{q=1}^{\nu'_{ip}} (c_{ip})_{(jq)_p} \right) \left(\Psi_i \prod_{p=1}^{L} \prod_{q=1}^{\nu'_{ip}} \Psi_{(jq)_p} \right) \tag{50}$$

such that, the mode strengths in the PC expansion for $\mathcal{R}^F = \sum_{a=0}^{P} \mathcal{R}_a^F \Psi_a$ are given by

$$\mathcal{R}_a^F = \sum_{i=0}^{P} \sum_{(j_b)_z=0}^{P} \left|_{b=1}^{\nu'_{iz}} \right|_{z=1}^{L} \left(k_i^F \prod_{p=1}^{L} \prod_{q=1}^{\nu'_{ip}} (c_{ip})_{(jq)_p} \right) \frac{\left\langle \Psi_a \Psi_i \prod_{p=1}^{L} \prod_{q=1}^{\nu'_{ip}} \Psi_{(jq)_p} \right\rangle}{\langle \Psi_a^2 \rangle} \tag{51}$$

It should be evident that proceeding in this manner is not only cumbersome but computationally intractable. This is a result of (1) the high-dimensional summation and product operations; (2) the fact that both the forward and reverse rates have complex dependencies on the presumed uncertainties in the reaction rate constants (preexponential, temperature exponent, and activation energy), field variables (temperature and concentrations), and thermodynamic properties; and (3) the necessary accounting for third body and pressure-falloff corrections. This is the primary motivation for the pseudospectral construction introduced above, and further specified below.

In the following, we discuss the dependence of the reaction rates on uncertain thermodynamic properties, and the specification of lognormal distributions for uncertain reaction rate parameters. Given this, we then proceed to the complete pseudo-spectral formulation for the chemical source term.

4.1.3 Reaction rates with thermodynamic uncertainties

The generalized source term allows any rate constant k_j^F to be uncertain. Consider a situation with several species $i = 1,\ldots,N$ participating in M reactions $k = 1,\ldots,M$ with forward rates $k_k^F = B_k T^{\alpha_1} e^{-E_k/T}$. The reverse rate is derived from the forward rate by a mutual relationship to the equilibrium constant. There may be instances where the mechanism specifies the reverse rate explicitly. If this is not the case, we must derive the spectral reverse reaction rate from the spectral forward rate constant. This coupling of forward and reverse reaction rates allows the introduction and propagation of thermodynamic parametric uncertainty into the source term.

The reverse rate is related to the forward rate through the equilibrium constant:

$$k_k^R = \frac{k_k^F}{K_{c,k}} \tag{52}$$

where $K_{c,k}$ is defined as:

$$K_{c,k} = \frac{e^{-\zeta_k/T}}{T^{\sigma_k}} \tag{53}$$

$$\sigma_k = \sum_{i=1}^{N} \nu_{ik} \tag{54}$$

$$\zeta_k = \sum_{i=1}^{N} \nu_{ik} g_i W_i \tag{55}$$

Note that $g_i = g_i(T) = h_i - Ts_i$ is the dimensionless Gibbs free energy per unit mass of species i.

The relationship between enthalpic and entropic uncertainties and the Gibbs free energy derives from the species heat capacity, $C_{p,i}$. Note that $g_i W_i = \overline{G}_i^o = G_i^o / RT_{\text{ref}}$ is the dimensionless per-mole Gibbs free energy, with G_i^o being the corresponding dimensional quantity. We recall that,

$$G_i^o = H_i^o - TS_i^o \tag{56}$$

Assuming ideal gas properties, one can compute the enthalpy and entropy by integration over T:

$$H_i^o = \int_0^T C_{p,i} dT \tag{57}$$

$$S_i^o = \int_0^T \frac{C_{p,i}}{T} dT \tag{58}$$

Let $C_{p,i} = C_{p,i}(T)$ be uncertain with a specified mean $C_{p,i0}$ and standard deviation $C_{p,i1}$,

$$C_{p,i} = C_{p,i0} + \xi_i C_{p,i1} \tag{59}$$

where $C_{p,i0} = C_{p,i0}(T)$ and $C_{p,i1} = C_{p,i1}(T)$ are known functions of temperature and ξ_i is a Gaussian random variable. Integrating to compute the enthalpy and entropy:

$$H_i^o = \int_0^T C_{p,i0} dT + \xi_i \int_0^T C_{p,i1} dT \tag{60}$$

$$= H_{i0} + \xi_i H_{i1} \tag{61}$$

$$S_i^o = \int_0^T \frac{C_{p,i0}}{T} dT + \xi_i \int_0^T \frac{C_{p,i1}}{T} dT \tag{62}$$

$$= S_{i0} + \xi_i S_{i1} \tag{63}$$

Reconstituting the definition of G_i^o, we have

$$G_i^o = H_{i0} + \xi_i H_{i1} - T(S_{i0} + \xi_i S_{i1}) \tag{64}$$

$$= H_{i0} - TS_{i0} + \xi_i (H_{i1} - TS_{i1}) \tag{65}$$

Substituting $\Psi_i = \xi_i$ (first-order modes in a Gaussian basis) and $\Psi_0 = 1.0$ gives a complete expression representing G_i^o in terms of the means and standard deviations of enthalpy and entropy:

$$G_i^o = (H_{i0} - TS_{i0})\Psi_0 + (H_{i1} - TS_{i1})\Psi_i \tag{66}$$

$$= \sum_{m=0}^{1} (H_{im} - TS_{im})\Psi_{m \cdot i} \tag{67}$$

G_i^o is then divided by $G_{\text{ref}} = RT_{\text{ref}}$ to nondimensionalize, and substitute into Eq. 55. Further, substituting ζ_k into Eq. 53, defines an uncertain $K_{c,k}$ in terms of uncertain thermodynamic parameters, coupling uncertainty in reaction equilibrium to uncertainty in the Gibbs free energy.

4.1.4 Lognormal distributions in a Gaussian basis

When assuming *a priori* the probability distribution corresponding to each uncertain reaction rate pre-exponential constant, it is necessary to choose distributions with zero probability of negative values. One typical choice is the lognormal distribution [27]. We address here the means of construction of a PC expansion for a random variable with a given lognormal distribution.

Let g be a Normal random variable with mean μ_g and standard deviation σ_g. Further, let u be a lognormal random variable [37], with

$$u = e^g \tag{68}$$

Then for a given $\zeta > 0$,

$$P[u \leq \zeta] = P[g \leq \ln \zeta] \tag{69}$$

Let the median of u be m_u, i.e. $P[u \leq m_u] = 0.5$. Then, since $P[g \leq \mu_g] = 0.5$, we have

$$\mu_g = \ln m_u \tag{70}$$

Following Phenix *et al.* [27], we can define a multiplicative factor, S, as

$$P[m_u/S \leq u \leq m_u S] = 1 - \varepsilon \tag{71}$$

where ε is a suitably small number (e.g. 0.05). then

$$\begin{aligned} 1 - \varepsilon &= P[u \leq m_u S] - P[u \leq m_u/S] = P[g \leq \ln(m_u S)] - P[g \leq \ln(m_u/S)] \\ &= P[g \leq \mu_g + \ln S] - P[g \leq \mu_g - \ln S] \\ &= 1 - P[g \geq \mu_g + \ln S] - P[g \leq \mu_g - \ln S] \end{aligned} \tag{72}$$

But, by the symmetry of g, $P[g \geq \mu_g + \ln S] = P[g \leq \mu_g - \ln S]$, hence

$$P[g \leq \mu_g - \ln S] = \frac{\varepsilon}{2} \tag{73}$$

and

$$P[g \leq \mu_g + \ln S] = 1 - \frac{\varepsilon}{2} \tag{74}$$

and, with U being the standard normal random variable, we have

$$P[g \leq \beta] \equiv F_g(\beta) = F_U(\frac{\beta - \mu_g}{\sigma_g}) \equiv P[U \leq \frac{\beta - \mu_g}{\sigma_g}] \tag{75}$$

thus,

$$P[g \leq \mu_g + \ln S] = F_U(\frac{\ln S}{\sigma_g}) = 1 - \frac{\varepsilon}{2} \tag{76}$$

and, from tabulated F_U, we have,

$$\frac{\ln S}{\sigma_g} = F_U^{-1}(1 - \frac{\varepsilon}{2}) \tag{77}$$

or,

$$\sigma_g = \frac{\ln S}{F_U^{-1}(1 - \frac{\varepsilon}{2})} \tag{78}$$

such that, e.g. for $\varepsilon = 0.05$, we have $F_U^{-1}(1 - \frac{\varepsilon}{2}) = 1.96$.

Thus, given a presumed lognormal distribution for the random variable u, with known mean m_u and multiplicative factor S, the corresponding normally distributed random variable g, such that $u = e^g$, is determined by its mean μ_g and standard deviation σ_g given in Eqs. 70 and 78 above, respectively. Given this, Ghanem [12] provides the requisite formulation for the mode strengths of the sought-after PC expansion for u, $u = \sum_0^P u_k \Psi_k$:

$$u_k = \exp[\mu_g + \frac{1}{2}\sigma_g^2]\frac{\sigma_g^k}{k!}. \tag{79}$$

4.1.5 Assembling a pseudospectral source term

As seen in the example of full-spectral reformulation, the evaluation of the products of multiple PC expansions can be quite complex. But by truncating the expansions of products to order P (section 2.2), a set of pseudospectral operators may be used to form the chemical source term.

First, define an overloaded product operator:

$$w = \prod_{i=1}^{N} {}^i u \approx \widetilde{w} = \prod_{i=1}^{N} {}^i u = {}^1u * {}^2u * {}^3u * \cdots * {}^N u \tag{80}$$

Using pseudospectral operators, the spectral source term can be constructed directly, following the definition in Section 4.1.

First, the forward reaction rate for each reaction,

$$k_k^F = B_k T^n e^{\frac{-E_a}{T}} \tag{81}$$

can be written in terms of pseudospectral multiplication, inversion, exponentiation, and logarithm operators:

$$k_k^F = B_k * (\exp[n * \ln(T) - E_a * (1 \oslash T)]) \tag{82}$$

where T is now a PC expansion for temperature, and B_k, n, and E_a are represented as PC expansions, introducing any specified parametric uncertainty.

Each reaction rate now includes the uncertainty contributed by an uncertain temperature (propagated from previous calculations), the parametric uncertainty that may be associated with a lognormally-distributed reaction preexponential, B_k, the parametric uncertainty in the activation energy, or parametric uncertainty in the temperature exponent n (each as specified).

The reverse rate can be calculated in two ways. If an explicit reverse reaction rate is available, it can be included directly. Or, the reverse reaction rate may be calculated from the equilibrium constant, Eq. 52, with the substitution of the appropriate pseudospectral operations and expanded variables and parameters. This computation also includes the effect of uncertain temperature itself, along with the derived uncertainty in Gibbs free energies, $g_i(T)$, due to dependence on the uncertain enthalpy and entropy.

The truncated stochastic expansion for the rate of progress of reaction k, $\mathcal{R}_k$, in terms of pseudospectral exponentiation operators ($**$) is then given by

$$\mathcal{R}_k = k_k^F * \prod_{i=1}^{N} c_i ** \nu'_{ik} - k_k^R * \prod_{i=1}^{N} c_i ** \nu''_{ik} \tag{83}$$

At this stage, third-body efficiencies may be added pseudospectrally (Eq. 33), with $C_k = 1$ for no correction and

$$C_k = \sum_{i=1}^{N} (\beta_{ik} * c_i) \tag{84}$$

for third-body corrections with no pressure fall-off. The implementation of pressure fall-off corrections follows in a very similar manner using pseudo-spectral operations.

The mass production rate (kg/m^3.sec) of species i is now written generally as

$$w_i = W_i \sum_{k=1}^{M} \nu_{ik} * C_k * \mathcal{R}_k \tag{85}$$

where w_i is a full stochastic expansion:

$$w_i = \sum_{k=1}^{P} w_{ik} \Psi_k \tag{86}$$

that can be implemented in the chemistry integration, or into any other operation that requires a stochastic chemical source term.

This functionality has been implemented in the form of a pseudospectral chemistry library that accepts a local chemical state vector and computes a spectral rate-of-progress for each reaction, based on the PC expansions for temperature and concentrations and the parametric uncertainty associated with enthalpies of formation, activation energies, exponents, and reaction preexponentials. This library returns a full PC expansion of the chemical source term for each individual species.

4.2 Extended ODE system

Returning to the governing equations for the chemical system, we write the PC expansions for concentrations, c_i, density, ρ, and temperature, T, as :

$$c_i(t) = \sum_{k=0}^{P} c_{ik}(t)\Psi_k, \quad i = 1,\ldots,N \tag{87}$$

$$\rho(t) = \sum_{k=0}^{P} \rho_k(t)\Psi_k \tag{88}$$

$$T(t) = \sum_{k=0}^{P} T_k(t)\Psi_k \tag{89}$$

and substitute into the corresponding chemical equations.

The time-evolution of the resulting pseudospectral chemical system is governed by the extended ODE system, for $k = 0,\ldots,P$:

$$\frac{dc_{ik}}{dt} = \frac{\mathrm{Da}}{W_i} w_{ik}, \quad i = 1,\ldots,(N-1) \tag{90}$$

$$\frac{d\rho_k}{dt} = \mathrm{Da} \sum_{i=1}^{N} \left\{ [1 \oslash (c_p * T)] * (h_i * w_i) \right\}_k - \frac{\mathrm{Da}}{W_i} \sum_{i=1}^{N} \left(\overline{W} * w_i \right)_k \tag{91}$$

The new algebraic constraints derive from mass conservation for mode 0 of the expansion, given that all higher-order modes sum to zero, since mass is conserved with zero-uncertainty, thus

$$\sum_{i=1}^{N} Y_{i0} = 1, \tag{92}$$

$$\sum_{i=1}^{N} Y_{ik} = 0, \quad k = 1,\ldots,P \tag{93}$$

and finally, from the perfect gas state equation, where P_0 is the stagnation pressure, assumed to be constant, and uncertain,

$$P_0 = \left[(\rho * T) \oslash \overline{W}\right]_0 \tag{94}$$

$$0 = \left[(\rho * T) \oslash \overline{W}\right]_k, \quad k = 1,\ldots,P \tag{95}$$

These equations are closed with deterministic initial conditions:

$$c_{ik}(t=0) = \begin{cases} c_i^0 & k = 0 \\ 0 & k = 1,\ldots,P \end{cases} \tag{96}$$

$$\rho_k(t=0) = \begin{cases} \rho^0 & k = 0 \\ 0 & k = 1,\ldots,P \end{cases} \tag{97}$$

4.3 Intrusive Results and discussion

4.3.1 Homogeneous ignition

To demonstrate the solution of the above UQ ODE model, we focused on the homogeneous constant-temperature ignition of a hydrogen-air mixture with a detailed chemical mechanism [34]. Initial conditions are deterministic, with T = 1200K, ρ = 0.276 kg/m^3, $c_{H_2} = 0.238 \times 10^{-5}$, $c_{O_2} = 0.119 \times 10^{-5}$, and $c_{N_2} = 0.832 \times 10^{-5}$. The integration proceeds at constant T and ρ. Physical properties, including the mean values of uncertain heats of formulation, were generated with the CHEMKIN properties database [30].

We specified two uncertain dimensions ($N_{\text{dim}} = 2$), and ran the integration with N_{ord} = 3, 5, and 7. We chose parametric uncertainties that reflect experimental uncertainties [27]. We modeled the uncertain pre-exponential Arrhenius rate constant for reaction 11 (HO_2 + H = OH + OH) as a lognormally distributed random variable, with a median value of 1.690×10^{14} mole-cm-sec-K and a multiplicative factor of 3.0. The second uncertain parameter is the enthalpy of OH, which we assume to have a normal distribution with a temperature-dependent mean given by the deterministic CHEMKIN [30] data base and a standard deviation of 0.01 kcal/mole [21,27].

The extended system of conservation equations with pseudospectrally-generated chemical source terms was integrated using the DVODE solver [29] with discretized Jacobians. The integration used a timestep of 2×10^{-4} ms. For the complete integration, the mean and standard deviation calculated at each N_{ord} varied by less than 0.5%. The results in this section use $N_{\text{ord}} = 5$.

Figure 11 shows the mean value of H_2O_2 concentration vs. time for the homogeneous ignition. Dashed lines indicate the range of resulting uncertainty with $\pm\sigma$ bounds. We observe a fast rise in both the mean H_2O_2 concentration and its standard deviation in the first 0.1 ms time interval. The resulting peak in uncertainty at $\approx$ 0.1 ms is a result of uncertainty in both the Rxn.11 rate constant and in the enthalpy of OH. At later time, there is a gradual decrease in uncertainty as the system tends towards equilibrium, where the rate-constant uncertainty would have no impact, while the enthalpic uncertainty would be reflected in the equilibrated species mixture.

Other radical species exhibit much larger uncertainties than H_2O_2. Figure 12 shows the mean value of HO_2 concentration vs. time, with $\pm\sigma$ bounds indicated. These results exhibit similar fast-rise in mean and standard deviation at early time, followed by a gradual decay to some asymptotically constant value of both at later time. Note the overall magnitude of total uncertainty in HO_2. Given realistic, moderate parametric uncertainties—uncertainties that reflect known limitations in the measurement of physical properties—the

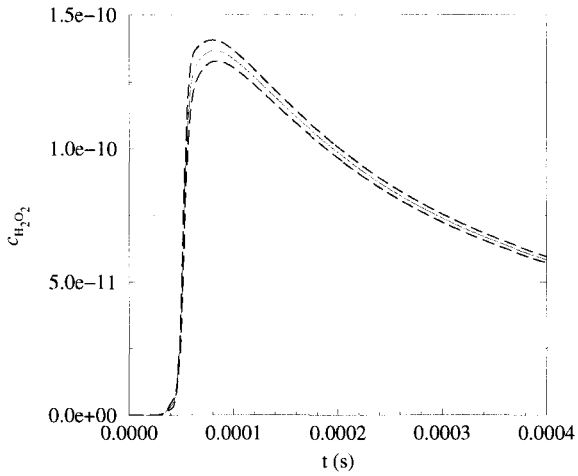

Figure 11: Mean value and uncertainty in the concentration of H_2O_2

standard deviation of the concentration reaches over 40% of the mean. We note that the uncertainty in the H_2O product (not shown) are relatively small, while that associated with some intermediate species is evidently quite large in comparison.

A notable strength of the polynomial chaos decomposition of uncertainty is that the contribution of specific parameters can be traced through each field quantity and into the simulation results. Figure 13 breaks down the 1^{st}-order contribution to the variance, σ^2, of the H_2O_2 concentration due to the two uncertain parameters. The shaded regions indicate the 1^{st}-order contribution of uncertainty from the uncertain enthalpy of formation, the 1^{st}-order contribution from the uncertain reaction preexponential, and the total variance calculated from the full expansion, include 2^{nd}, 3^{rd}, and higher-order effects. For these two uncertain parameters, the resulting concentration PDFs are roughly Gaussian in form, leading to higher-order contributions that are small compared to the standard deviation. Other studies that studied additional uncertain parameters [21] have shown larger contributions from higher orders. This form of analysis has great utility in larger and more complex systems, designating where, and to what extent, a given parametric uncertainty affects the total uncertainty in the predictions. This specifies which parameters are most impacted by experimental limitations, and thus may be used to guide future research. Also, since approximations and reductions are present in many chemical models, this methodology may reveal inherent limitations of mechanisms that may not be robust predictors of concentrations of intermediate radical species.

4.3.2 Solvability of the pseudospectral formulation

A larger goal of this intrusive UQ construction is to construct large-scale reacting-flow simulation codes using pseudospectral stochastic PC operations. With this in mind, the solvability of the stiff chemistry may shed light into the numerical difficulties that may be encounted in more complex, highly-coupled multidimensional solvers. Two related effects are most apparent when assessing the solvability of the homogeneous ignition problem—the ability of the intrusive polynomial chaos approach to adequately represent the evolving probability distributions of the system variables, and the magnitude of the uncertainty.

Fig. 14 compares the PDFs of c_{HO_2} expanded to third, fifth, and seventh order at $t = 3.6 \times 10^{-5}$ s, using the pseudospectral source term, in the region of maximum uncertainty. The shape of the PDF is not skewed greatly from a Gaussian, but the standard deviation is considerable and the coefficient of variation, $C = \sigma/c_i^0$, becomes quite large. There are clear discontinuities/spikes/artifacts in the PDF for $N_{\text{ord}} = 3$ (solid line), indicating that third-order expansions insufficiently resolve the shape of the distribution. PDFs at $N_{\text{ord}} = 5$ and 7 (circles and squares, respectively) show smoothly-varying distributions. These discontinuities reflect large values present in the highest modes of expansion. In this example, the third-order modes of the third-order expansion achieve the same overall magnitude as the first-order modes, resulting in an PC expansion

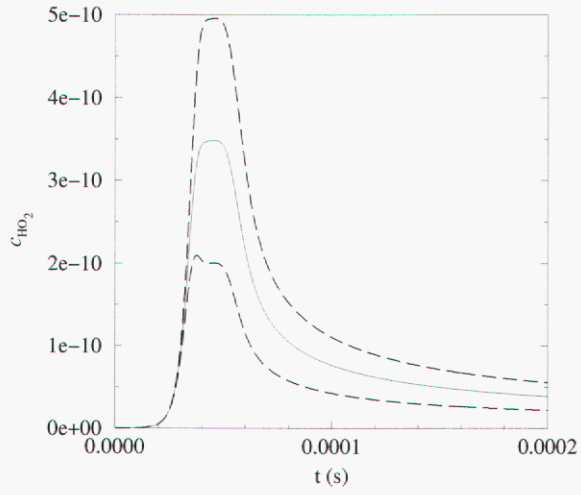

Figure 12: Mean value and uncertainty in the concentration of HO_2

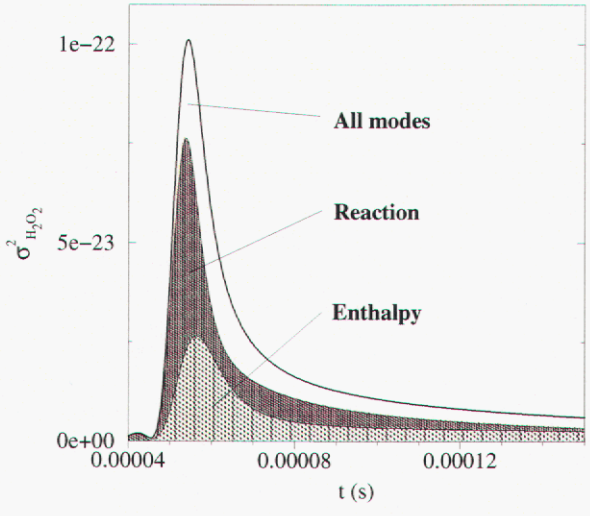

Figure 13: Decomposition of the uncertainty in H_2O_2

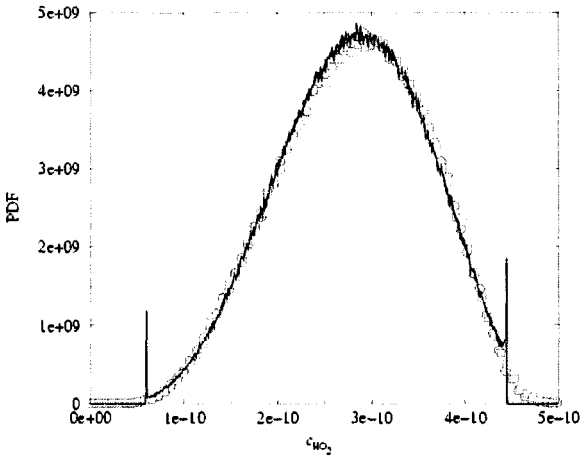

Figure 14: PDFs of HO_2 concentration at $t = 3.6 \times 10^{-5}$ s. The solid line represents $N_{\text{ord}} = 3$, the circles $N_{\text{ord}} = 5$, and the squares $N_{\text{ord}} = 7$

that is not convergent.

With the basic physical constraint of positive values for concentration, the resolution of the PDF near zero becomes important. Recall that the reformulation replaces each random variable/process by a spectral PC expansion. While we do not discretize the PDF itself, a non-convergent expansion, i.e. one in which significant energy exists in the neglected/truncated higher order modes, will result in an unacceptable probability density. PDFs that are poorly resolved and non-convergent expansions lead to large errors in the computed solution, and can lead to instabilities in the time integration procedure.

Figure 15 compares the PDF of c_{HO_2} at several points in the ignition process ($N_{\text{ord}} = 5$). As seen in Fig. 12, during the initial ignition, total uncertainty increases rapidly, with the standard deviation attaining a similar order-of-magnitude to the mean. When mode 1, which here dominates the standard deviation of the distribution, exceeds 30% of the mean, a steeply-varying PDF is required to insure no significant probability of negative c_{HO_2} values. As very large uncertainties develop, and σ approaches the mean, larger N_{ord} may be needed to compensate, and to adequately resolve the energy within the truncated expansion. This increases the complexity and the computational effort required to solve the problem.

Figure 16 illustrates the magnitude of mode strengths for HO_2 concentration for the PDF at $t = 3.8 \times 10^{-5}$ s, including expansions truncated at N_{ord} =3, 5, and 7. Vertical bars group the modes $|c_k|$ by order, from 1^{st} to 7^{th}. For $N_{\text{ord}} = 3$ and $N_{\text{ord}} = 5$, we see that some modes within the highest order bracket are greater in magnitude than the corresponding modes for the higher-order expansions. However, the trend of the modes in the log-linear plot suggests a trend toward convergence. In this plot, the maximum and minimum mode amplitudes for each order correspond to modes dependent only on one of the uncertain dimensions. If we plot these values vs. N_{ord}, a roughly linear decay that suggests exponential convergence, with the maximum amplitudes (dependent on reaction uncertainty) converging more slowly than the minimum amplitudes (dependent on enthalpic uncertainty).

As the standard deviation of the PDF increases, the behavior of the PDF tails around $c_i = 0$ becomes an issue. If indeed the pseudospectrally-reformulated problem acts upon the full distribution of possible concentrations (as well as temperatures, densities, etc.), we should expect that finite probabilities of unphysical negative concentrations, generated by insufficiently-resolved stochastic space near $c_i = 0$, will cause the integration to fail.

To illustrate this, we performed another calculation of an extreme case. In the case of large uncertainties in specific parameters or a large number of independent uncertainty parameters, a large total uncertainty may be generated. Figure 17 shows the PDFs of $c_{H_2O_2}$ at several times for an alternate ignition computation. For this case, performed at $N_{\text{ord}} = 5$, we set the preexponential of reaction 1 ($H+O_2=O+OH$) to be uncertain with a $S = 1.5$ in addition to the previously-specified $S = 3.0$ for reaction 11. The enthalpic uncertainty was removed, leaving $N_{\text{dim}} = 2$. This generates a much greater total uncertainty through direct generation by the source term

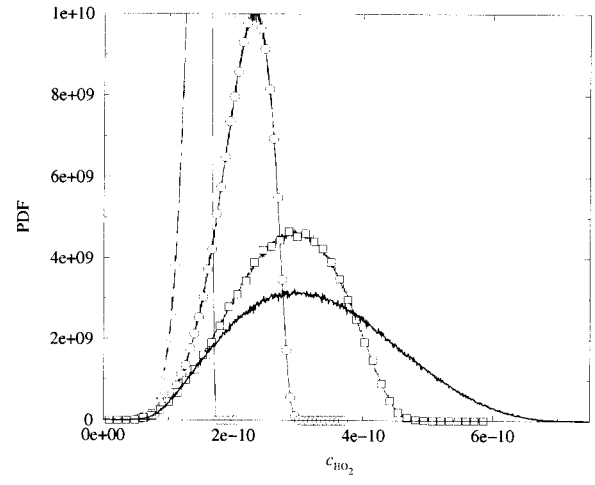

Figure 15: PDFs of HO_2 concentration at $t = 3.2 \times 10^{-5}$ s (diamonds), 3.4×10^{-5} s (circles), 3.6×10^{-5} s (squares), and 3.8×10^{-5} s (solid line).

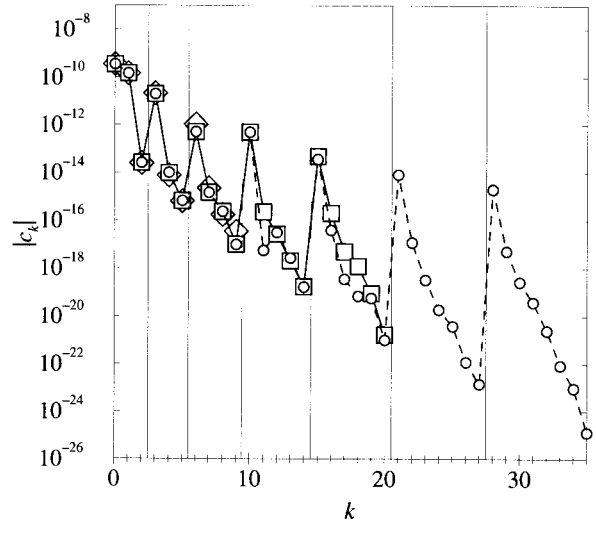

Figure 16: Absolute magnitude of $c_{HO_2}(k)$ modes at maximum total c_{HO_2} uncertainty for $N_{ord} = 3$ (diamonds), $N_{ord} = 5$ (squares), and $N_{ord} = 7$ (circles). Vertical lines separate orders from first through seventh.

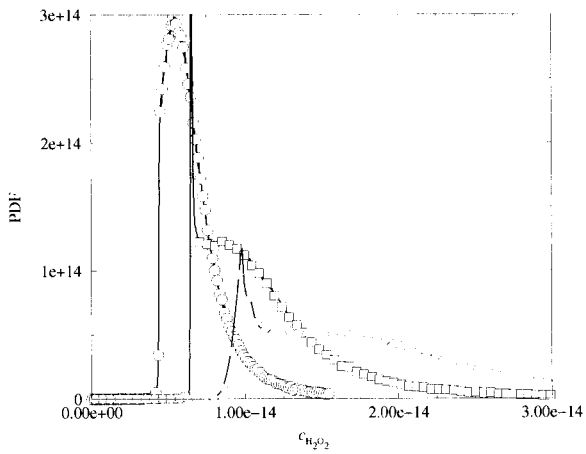

Figure 17: PDFs of H_2O_2 concentration at $t = 1.6 \times 10^{-5}$ s (circles), 1.8×10^{-5} s (squares), and 2.0×10^{-5} s (diamonds).

and through the interactions between two large uncertain parameters. The PDFs grow rapidly in width, with the standard deviation approaching the mean and signs of clear nonconvergence of the PC expansions after 1.8×10^{-5} s. Analysis of the individual PC modes indicates that once a concentration PDF extends into the nonphysical $c_j < 0$ region, the values of the modes diverge rapidly and the time integration fails. In Fig. 18 a plot of mean concentration and standard deviation vs. time is overlaid with individual 1^{st} and 2^{nd}-order mode values. Vertical dashed lines notes the three timesteps referenced in Fig. 17. By $t = 2.0 \times 10^{-5}$ s, the standard deviation has exceeded the mean, and both 1^{st} and 2^{nd}-order modes are growing rapidly, resulting in failure of the integration at $t = 2.75 \times 10^{-5}$ s.

4.3.3 Model initial-value problem

To better understand the consequences of large standard deviations with a mean near-zero, i.e. a large coefficient of variation (COV), we considered a simpler case–the time integration of a model initial-value problem based on the chaos system. It is important to address and explore the conditions that lead to very fast growth of the solution and potential instability, as can happen during homogeneous ignition with large uncertainties.

Consider first the ODE given by

$$\frac{du}{dt} = g(u) = au(u+b)(u+c) \tag{98}$$

with $u(t=0) = U$, which has two attractors, at $u = -b$ and $-c$. It also has a saddle point at $u = 0$. Using values of the constants of $b = 10$, $c = -1$, $a = -1$, any trajectory with $U > 0$ is attracted to the $u = 1$ limit, while $U < 0$ trajectories are attracted to $u = -10$. A trajectory with $U = 0$ remains at $u = 0$.

Now, allow u to be a stochastic quantity, $u = \sum_{k=0}^{P} u_k \Psi_k$, using fourth-order chaos ($P = 4$), and let the constants a, b, c be deterministic as chosen, but let the initial condition U have a specified uncertainty, given by a mean U_0 and a standard deviation U_1, and a presumed Normal distribution. Thus, $U = U_0 + U_1 \xi$, with zero higher order modes.

Given U_1, consider the behavior of $u_0(t)$ for two different values of $U_0 = 0.2, 0.3$. The corresponding PDFs for U are shown in Fig. 19. While both have non-zero probability of negative values–given the infinite support of the gaussian distribution, the case with $U_0 = 0.2$ has a larger COV, with corresponding larger probability of negative U. As Fig. 20 shows, the time evolution of u_0 is drastically different for the two cases. The initial stage of the evolution (up to $\sim t = 0.6$) is towards the positive attractor in both cases, with only minor difference in the trajectories. Soon after this however, the case with larger negative overlap is attracted towards the negative stationary point. The end result at $t = 1.5$ is that the two cases are stationary at the two attractors.

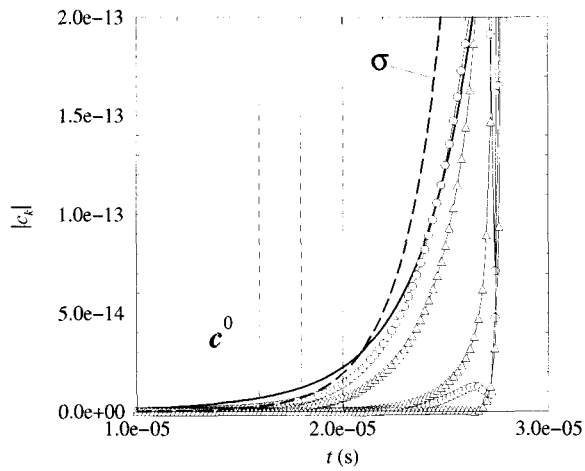

Figure 18: Evolution of mean $c_{H_2O_2}$ (solid line), first order $c_{H_2O_2}$ modes (circles), second-order $c_{H_2O_2}$ modes (triangles), and standard deviation (dashed line) vs. time. Vertical dashed lines correspond to the times illustrated in the previous figure.

We note of course, that there is no sampling of either PDF in the time integration procedure. The equations integrated are the Galerkin-projected ODEs for the polynomial chaos expansion mode strengths. These equations are representing the physical situation accurately, thereby reflecting the increased probabilitiy of negative samples and its consequences. Also note that, despite the small probability of negative initial values, the mean of the PDF is completely dominated by their large magnitude as they tend towards -10, versus the much smaller values of the samples attracted to the positive limit.

We also note that, with an alternative problem, e.g. $du/dt = -10u(u-1)$, which has attractors at $u = 1$ and $-\infty$, the negative overlap of the PDF of U is a source of instability, as the negative branch of the solution tends to $-\infty$. The infinite well of this attractor creates a potential source of instability, as any overlap of the solution PDF with the region $u < 0$ would allow the solution to grow without bounds. A normally distributed initial condition can lead to an infinite rate of growth of the solution if its COV is large-enough.

Moreover, note that even the stable initial conditions in this discussion are in fact unstable if sufficiently high order is used for the PC expansion. For example, while using a 7^{th}-order expansion, still gives the same final limit of 1.0 for u_0 in the $U_0 = 0.3$ case, taking the order up to 11 leads to u_0 heading into negative territory after first approaching 1.0. The higher accuracy with the higher-order expansions leads to adequate resolution of the very small negative tail region in the $U_0 = 0.3$ case, and therefore the attraction of the mean to the large negative limit. The infinite support of the Gaussian PDF of the normally-distributed initial condition implies that, in the limit of infinite order, any such initial condition will tend to the negative limit. It is only the inaccuracy of the low-order expansions that prevents this from ocurring for some small COV values ($< 0.08/0.3$).

It is also noteworthy that this same dependence on PC order and COV is observable with an initial condition U that is lognormally distributed. Thus, for example, we find that with a median U of 0.3, and a multiplicative factor $S_U = 4.5$, while both 4^{th} and 7^{th}-order computations of u_0 reach the positive limit and stay there within the 1.5 time limit, using 11^{th}-order chaos we find that u_0 leaves the 1.0 stationary point at around $t = 1.4$ and heads downward. Further, going to $S_U = 5.4$, we find that this occurs earlier at $t = 1$, and u_0 reaches the negative stationary point by $t = 1.5$. Moreover, with $S_U = 9$, even the 4^{th}-order solution leaves positive territory around t=0.5, and decreases towards -10. While this may seem surprising at first glance, given that the initial PDF ought-not to have any negative part, the explanation is based on the inadequate resolution of this and later PDFs by the truncated PC expansion. In the limit of very large S_U/U_0, or very low order, the truncated PC expansion for the lognormally distributed U exhibits an actual PDF that does have a finite probability of negative values. For example, for $S_U = 9$, the 4^{th}-order PDF of U has significant probabilities of negative values. This is not so at the lower S_U values ($S_U = 4.5 - 5.4$), where the initial PDFs are indeed

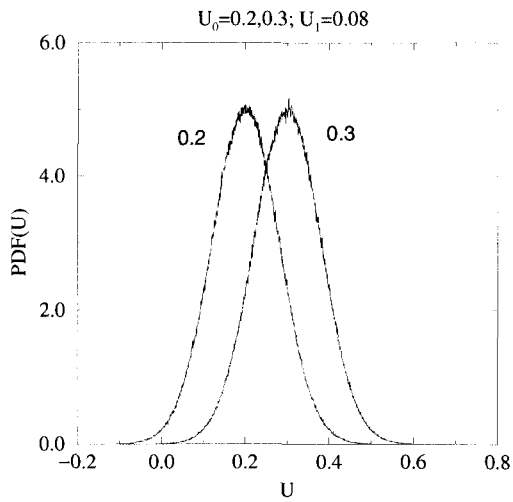

Figure 19: Two initial PDFs with $U_0 = 0.2$, and $U_0 = 0.3$, and $U_1 = 0.08$ in both cases. The PDF with the mean closer to zero overlaps the negative U region.

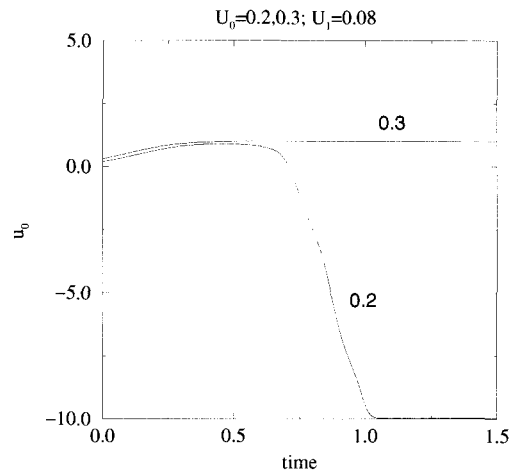

Figure 20: Evolution of u for each of the initial PDFs in Fig. 25, with $du/dt = au(u+b)(u+c)$ as defined above. The case with the initial PDF overlapping zero is attracted to the negative stationary point, in contrast to solution with an initial PDF that has much smaller overlap with zero.

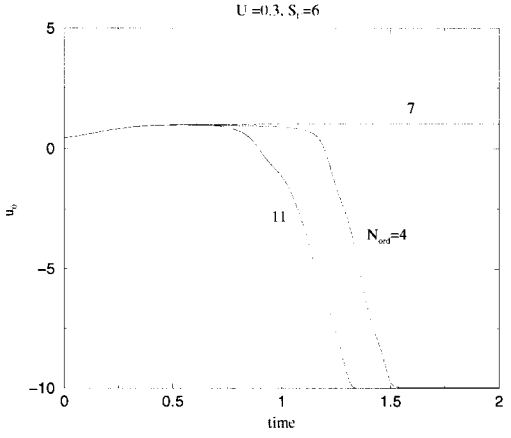

Figure 21: Evolution of u for a lognormal initial condition with increasing polynomial chaos order N_{ord}.

well resolved with the PC expansions with order ≥ 4. However, the time integration procedure with the 11^{th}-order expansion leads to finite probabilities of negative $u(t)$ at early time, which tends to dominate the solution, driving u_0 to the negative limit. In fact, the results shown in Fig. 21, for $S_U = 6$, illustrate this situation very clearly. The results show that increasing the PC order from 4 to 7 leads to the stabilization of the solution at the positive attractor (at least up to $t = 2.0$). On the other hand, increasing the order further, to 11, leads back to an early departure of the solution from the positive limit.

We note finally that the implications of negative PDF tails are crucially important for stable integration of the chemical system. Finite probabilities of negative concentrations, temperature, or density, can cause destabilization of the time integration procedure. We do observe that at high-enough uncertainty in rate constants such instabilities do occur, as observed earlier above.

Finally, it is important to examine clues for impending instability in the time integration due to such negative tails. Examining the system jacobian eigenvalue evolution does not give immediate clues to stability, as both the finite and infinite attractor problems exhibit rapidly-growing positive maximum eigenvalues for $C_U > 0.3 - 0.4$. Additional analysis needs to be done to establish metrics for judging stability. This is investigated in the sections below.

4.3.4 Stochastic inversion

An interesting approach for detecting that a stochastic quantity u has a finite probability of crossing zero is to evaluate its stochastic inverse and examine the condition number of the matrix involved. This reveals one possible pathway to numerical difficulties—for example when part of the PDF for density, ρ, closely approaches zero, can we then expect to evaluate the stochastic inverse $T = 1/\rho$? In fact, this effect is observed during hydrogen-air ignition studies—the T expansion resulting from an inversion of density contains a small but finite probability of extremely large values. We present here the means of doing this check.

Note that we use a linear system solution to find the stochastic inverse, as outlined in [20, 24]. We outline that procedure here in order to explain the zero-crossing detection strategy. Thus, first, define the PC expansion for the random quantity u, and its inverse v,

$$u = \sum_{i=0}^{P} u_i \Psi_i \tag{99}$$

$$v = \frac{1}{u} = \sum_{j=0}^{P} v_j \Psi_j. \tag{100}$$

Then, since $w = uv = 1$, we express the PC expansion for the product,

$$w = \sum_{q=0}^{P} w_q \Psi_q = uv = \sum_{j=0}^{P} \sum_{i=0}^{P} u_i v_j \Psi_i \Psi_j. \tag{101}$$

Using Galerkin projection, we express the coefficients of the expansion for w in terms of the coefficients u_i and v_j,

$$w_k = \sum_{j=0}^{P} \sum_{i=0}^{P} u_i v_j \frac{< \Psi_i \Psi_j \Psi_k >}{< \Psi_k^2 >} = \sum_{j=0}^{P} \sum_{i=0}^{P} u_i v_j C_{ijk} \tag{102}$$

But, since $w_k = \delta_{k0}$, we have

$$\sum_{j=0}^{P} \sum_{i=0}^{P} u_i v_j C_{ij0} = 1 \tag{103}$$

$$\sum_{j=0}^{P} \sum_{i=0}^{P} u_i v_j C_{ijk} = 0 \qquad k = 1, \cdots, P \tag{104}$$

This is a $(P+1)$-dimensional system of linear equations for v_j, $j = 0, \cdots, P$, i.e.,

$$\mathbf{A}\mathbf{v} = \mathbf{b} \tag{105}$$

In the $\mathbf{A}$-matrix, the entry for row $k = 0, \cdots, P$ and column $j = 0, \cdots, P$ is given by

$$A_{kj} = \sum_{i=0}^{P} u_i C_{ijk} \tag{106}$$

and entries for the right-hand side are given by

$$b_k = \delta_{k0}, \quad k = 0, \cdots, P \tag{107}$$

Note that A_{kj} is simply a linear combination of the modes of u, and thus easily evaluated. We can thus compute the condition number of $\mathbf{A}$ (the ratio of its maximum and minimum eigenvalues). Condition numbers of order 1 indicate a readily-invertable distribution, while larger condition numbers reflect potential difficulties with the inversion, and potential incidences of zero crossing in the PDF of u.

4.3.5 Detecting negative PDF tails

The stochastic natural logarithm function can be used to detect negative values in tails of distributions. Let u be a normal distribution with COV C_U, $u = \mathcal{N}(\sigma/C_U, \sigma)$, then fix σ and vary C_U. For each such choice of u, evaluate the error $\mathcal{E}$ given by

$$\mathcal{E} = ||u - \exp(\ln(u))||_\infty \tag{108}$$

The variation of E with COV is shown in Fig. 22. The error is small and smoothly varying for $C_U < 0.36$. It also decays with decreasing C_U. For $C_U > 0.36$, however, the error is large, roughly fixed, and non-smooth. At large COVs, the PDF of u is wide enough to have $3\sigma > \mu$, leading to finite probability of negative u values. Clearly, the ln()-function evaluation with polynomial chaos will fail when the PDF has a significant negative tail.

These results suggest the potential utility of the stochastic ln()-function for monitoring the solution during a time integration procedure, and providing early detection of signs of trouble. This information could be used to periodically filter the solution, sacrificing some measure of accuracy for stability.

4.4 Intrusive UQ Summary

A generalized intrusive spectral projection scheme has been presented and implemented for detailed chemistry. We presented both fully spectral and pseudospectral constructions. We examined a chemical system

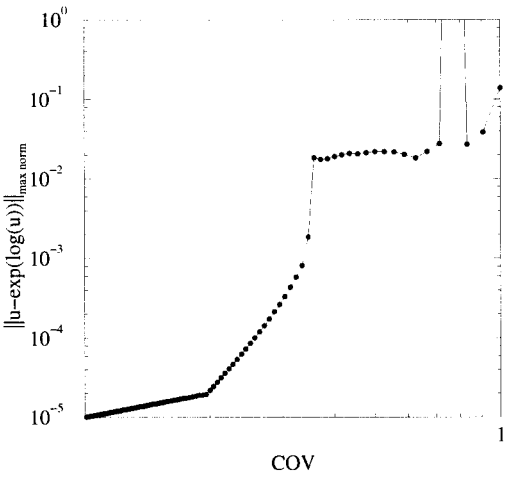

Figure 22: Computed error $||u - exp(log(u))||_\infty$ versus C_u, where $u = \mathcal{N}(0.2/C_u, 0.2)$ using fourth order chaos.

with only two uncertain parameters and moderate uncertainties. The hydrogen combustion model amplified this parametric uncertainty considerably in some of the radical species. The amplification of small uncertainties in this fashion may call into question the robustness of a model for predictions of a specific species, and highlights the importance of including uncertainty quantification in computations.

A full multiparameter analysis would include known uncertainties in empirically-determined enthalpies of formation, and reaction rate preexponentials. Future studies using this method will investigate the cumulative effects of such multi-parameter systems, particularly those including transport, focusing on the higher-order effects caused by the inherent coupling of the stochastic variables.

Limitations of the method include considerations of the resolution of the stochastic space. For example, the constraint $c_j > 0$ within the chemistry integration may require high-order expansions (representing skewed or sharply-defined PDFs) to ensure convergent expansions with a HERMITE basis. Unphysical PDFs or non-convergent expansions may be corrected via the use of higher-orders, with the corresponding computational expense of a greater number of simultaneous equations. On the other hand, stability is not guaranteed for arbitrarily high orders, as indicated by the above model-problem results. Alternatively, filtering of the PC expansions to decrease the amplitude of higher-order modes may be sufficient to stabilize the computations. More work is required in this regard.

5 Conclusions

This work has covered a wide range of issues pertaining to the quantification of uncertainty propagation in models of reacting thermofluid systems. We have presented both intrusive and non-intrusive UQ constructions based on spectral and pseudo-spectral polynomial chaos expansions. We have applied these constructions to chemically reacting flow systems, allowing for uncertain reaction rate and thermodynamic parameters. While not presented here, we have also developed elsewhere similar implementations for flow in heated cavities [24]. We have also applied the intrusive pseudo-spectral construction to a multi-dimensional low Mach number reacting flow system.

It is clear that where model-reformulation, and therefore code rewrite, is feasible, and where model non-linearities are not excessive, the intrusive construction is superior in terms of computational efficiency. Dealing with chemical systems however, non-linearities are by no means weak, and the present intrusive construction faces many challenges. These continue to be the subject of ongoing research, focusing on methods for filtering the spectral expansions, and/or choosing alternate PC bases in place of the Hermite-Gaussian combination.

Where legacy code rewrite is not feasible, or extreme non-linearities hinder the intrusive approach, the non-intrusive construction is necessary. However, it is clear that monte-carlo/latin-hypercube sampling strategies, which typically require many thousands of samples, are not practical for large-scale computations. Alternate, more efficient, sampling techniques are needed. Given that the sampling problem is essentially an N_{dim}-dimensional integration problem, advanced quadrature techniques can potentially alleviate the problem and allow reduced numbers of samples. Specifically, we have found that for a small number of dimensions ($N_{\text{dim}} \leq 3$), Gauss-Hermite quadrature provides a much more efficient sampling strategy than latin-hypercube. However, the curse of dimensionality catches up with this technique when N_{dim} reaches $O(10)$. In this limit, we see great potential in the use of cubature/sparse-quadrature techniques. These advanced sampling techniques are a subject of ongoing work.

Acknowledgements

This work is supported through the Laboratory Directed Research and Development program at Sandia National Laboratories funded by the U.S. Department of Energy, and by the DOE Office of Basic Energy Sciences (BES), Division of Chemical Sciences, Geosciences and Biosciences.

References

[1] Wiener, N., *Amer. J. Math.*, 60:897–936 (1938).

[2] Cameron, R.H., and Martin, W.T., *Ann. Math.*, 48:385–392 (1947).

[3] Chorin, A.J., *J. Computational Phys.*, 8:472–482 (1971).

[4] Maltz, F.H., and Hitzl, D.L., *J. Computational Phys.*, 32:345–376 (1979).

[5] Meecham, W.C., and Jeng, D.T., *J. Fluid Mech.*, 32:225 (1968).

[6] Chorin, A.J., *J. Fluid Mech.*, 63:21–32 (1974).

[7] Ghanem, R.G., and Spanos, P.D., *Stochastic Finite Elements: A Spectral Approach*, Springer Verlag, New York, (1991).

[8] Ghanem, R., *Comput. Methods Appl. Mech. Engrg.*, 158:199–220 (1998).

[9] Ghanem, R., *Comput. Methods Appl. Mech. Engrg.*, 168:19–34 (1999).

[10] Ghanem, R., *ASCE J. Eng. Mech.*, 125:26–40 (1999).

[11] Ghanem, R.G., Red-Horse, J.R., and Sarkar, A., *8th ASCE Specialty Conference of Probabilistic Mechanics and Structural Reliability*, ASCE, (2000).

[12] Ghanem, R.G., *ASME J. Appl. Mech.*, 66(4):964–973 (1999).

[13] Sakamoto, S., and Ghanem, R.G., *ASCE J. Eng. Mech.*, 128(2):190–201 (2002).

[14] Le Maître, O.P., Knio, O.M., Najm, H.N., and Ghanem, R.G., *J. Comp. Phys.*, 173:481–511 (2001).

[15] Le Maître, O.P., Reagan, M.T., Najm, H.N., Ghanem, R.G., and Knio, O.M., *J. Comp. Phys.*, 181:9–44 (2002).

[16] Xiu, D., Lucor, D., Su, C.-H., and Karniadakis, G.E., *ASME J. Fluids Engineering*, 124:51–59 (2002).

[17] Xiu, D., and Karniadakis, G.E., *SIAM J. Sci. Comput.*, 24(2):619–644 (2002).

[18] Xiu, D., and Karniadakis, G.E., *Computer Methods in Applied Mechanics and Engineering*, 191:4927–4948 (2002).

[19] Debusschere, B., Najm, H., Matta, A., Shu, T., Knio, O., Ghanem, R., and Le Maître, O., *Proc. 5^{th} Int. Conf. on Modeling and Simulation of Microsystems*, pp. 384–387, (2002).

[20] Debusschere, B.J., Najm, H.N., Matta, A., Knio, O.M., Ghanem, R.G., and Le Maître, O.P., *Phys. Fluids*, 15(8):2238–2250 (2003).

[21] Reagan, M.T., Najm, H.N., Ghanem, R.G., and Knio, O.M., *Combustion and Flame*, 132:545–555 (2003).

[22] McKay, M.D., Beckman, R.J., and Conover, W.J., *Technometrics*, 21:239–245 (1979).

[23] Schoutens, W., *Stochastic Processes and Orthogonal Polynomials*, Springer, (2000).

[24] Le Maître, O.P., Reagan, M.T., Debusschere, B.D., Najm, H.N., Ghanem, R.G., and Knio, O.M., *SIAM J. Scientific Computing* (2003) submitted.

[25] Debusschere, B.J., Najm, H.N., Pebay, P.P., Knio, O.M., Ghanem, R.G., and Le Maître, O.P., *SIAM J. on Sci. Comp.* (2003) submitted.

[26] Tester, J.W., Holgate, H.R., Armellini, F.J., Webley, P.A., Killilea, W.R., Hong, G.T., and Barner, H.E., Emerging technologies for hazardous waste management, American Chemical Society, (1993).

[27] Phenix, B.D., Dinaro, J.L., Tatang, M.A., Tester, J.W., Howard, J.B., and McRae, G.J., *Combustion and Flame*, 112:132–146 (1998).

[28] Isukapalli, S.S., Roy, A., and Georgopoulos, P.G., *Risk Analysis*, 18(3):351–363 (1998).

[29] Brown, P.N., Byrne, G.D., and Hindmarsh, A.C., *SIAM J. Sci. Stat. Comput.*, 10:1038–1051 (1989).

[30] Kee, R.J., Rupley, F.M., and Miller, J.A., Sandia Report SAND89-8009B, Sandia National Labs., Livermore, CA, (1993).

[31] Kee, R.J., Grcar, J.F., Smooke, M.D., and Miller, J.A., Sandia Report SAND85-8240, Sandia National Labs., Livermore, CA, (1993).

[32] Eldred, M.S., Technical report, Sandia Technical Report SAND98-0340, (1998).

[33] Wojtkiewicz, S.F., Eldred, M.S., Field, R.V., Urbina, A., and Red-Horse, J.R., *Proceedings of the 42nd AIAA/ASME/ASCE/AHS/ASC Structures, Structural Dynamics, and Materials Conference*, (2001).

[34] Yetter, R.A., Dryer, F.L., and Rabitz, H., *Combust. Sci. Technol.*, 79:97 (1991).

[35] Holgate, H.R., and Tester, J.W., *Combust. Sci. Technol.*, 88:369 (1993).

[36] Najm, H.N., Wyckoff, P.S., and Knio, O.M., *J. Comp. Phys.*, 143(2):381–402 (1998).

[37] Vanmarcke, E., *Random Fields: Analysis and Synthesis*, MIT Press, (1988).

Distribution

Printed copies sent through the mail

1		Prof. Omar M Knio Dept. of Mechanical Engineering 103 Latrobe Hall The Johns Hopkins University Baltimore, MD 21218-2686
1		Prof. Ahmed Ghoniem MIT, Rm 3-342 77 Mass Ave. Cambridge, MA 02139
1		Prof. Tarek Echekki Mechanical and Aerospace Engineering 4152 Broughton Hall 2601 Stinson Drive North Carolina State University Raleigh, NC 27695-7910
1		Prof. Roger Ghanem Dept. of Civil Engineering The Johns Hopkins University Baltimore, MD 21218-2686
1		Prof. Olivier Le Maitre Universite d'Evry Val d'Essonne Centre d'Etudes de m'ecanique d'Ile de France 40 rue du Pelvoux CA 1455 91020 Evry cedex France
20	MS9051	Habib N. Najm
1	MS0188	Donna Chavez - LDRD Office
1	MS0847	Steve Wojtkiewicz
1	MS0828	John Red-Horse
1	MS9042	Christopher Moen
1	MS9051	Andrew McIlroy
3	MS9018	Central Technical Files, 8945-1
1	MS0899	Technical Library, 9616
1	MS9021	Classification Office, 8511/Technical Library, MS 0899,9616 DOE/OSTI via URL

This page intentionally left blank